Deep continental roots and cratons

D. Graham Pearson[1], James M. Scott[2], Jingao Liu[3], Andrew Schaeffer[4], Lawrence Hongliang Wang[5], Jeroen van Hunen[6], Kristoffer Szilas, [7], Thomas Chacko[1], Peter B. Kelemen[8]

1) Department of Earth & Atmospheric Sciences, University of Alberta, Edmonton, Alberta, Canada, T6G 2E3.
2) Department of Geology, University of Otago, PO Box 56, Dunedin 9054, New Zealand
3) State Key Laboratory of Geological Processes and Mineral Resources, China University of Geosciences, Beijing 100083, China.
4) Geological Survey of Canada, Pacific Division, Natural Resources, Sidney, BC, Canada
5) Institute for Energy Technology, Instituttveien 18, 2007 Kjeller, Norway
6) Department of Earth Sciences, Durham University, South Road, Durham DH1 3LE, United Kingdom
7) Department of Geosciences and Natural Resource Management, University of Copenhagen, Øster Voldgade 10, 1350 København, Denmark
8) Lamont-Doherty Earth Observatory, Columbia University, Palisades, NY 10964-8000, USA

Main Text 5494 Words

Summary:

The formation and preservation of cratons - the oldest parts of the continents comprising over 60% of the continental landmass - remains an enduring problem. Key to craton development is how and when the thick strong mantle roots that underlie these regions formed and evolved. Peridotite melting residues forming cratonic lithospheric roots mostly originated via relatively low-pressure melting and were subsequently transported to greater depth by thickening produced by lateral accretion and compression. The longest-lived cratons assembled during Mesoarchean and Paleoproterozoic times, creating the 150 to 250 km thick, stable mantle roots that are critical to preserving Earth's early continents and central to defining the cratons although we extend the definition of cratons to include extensive regions of long-stable Mesoproterzoic crust also underpinned by thick lithospheric roots. The production of widespread thick and strong lithosphere via the process of orogenic thickening, possibly in several cycles, was fundamental to the eventual emergence of extensive continental landmasses - the cratons.

[158 Words]

1. The lithospheric mantle – a brief introduction

The outer highly viscous "skin" of the Earth - the lithosphere - separates the surface from its interior. Lithosphere definitions have many nuances[1]. Here, we define the lithosphere simply as Earth's strong outer thermal boundary layer through which heat is primarily transferred by conduction (**Box 1**). The base of the lithosphere can be defined as the point at which a linear extrapolation of this conductive geotherm intersects the mantle isentrope. The cooler temperatures and higher viscosities of lithosphere compared to underlying asthenospheric mantle contribute to it being one of the longest-lived large-scale features of the solid Earth. The mantle portion of the lithosphere, the "mantle root", is generally thicker and older beneath continents than oceans[2].

Given the controversies surrounding the origin of the crust that we walk on and sample readily as geologists, it should not surprise the reader that the origin of the deeper parts of the solid Earth, such as the continental lithospheric mantle, is as controversial and more difficult to constrain. Here, we review some physical and chemical properties of deep lithospheric roots beneath continents and examine their integral role in forming the oldest parts of the continents - the cratons. We explore how these properties arose in the context of mantle melting environments. The melting ages of peridotites forming the cratonic roots, and their temporal relationship with the overlying crust are examined before using geodynamic models to constrain the origin of the large-scale geological characteristics of cratons, i.e., how the cratons were made.

2. Making cratons and their lithosphere

2.1. Defining a craton

Despite lithospheric mantle comprising up to 80% of the thickness of continental plates, the origin and evolution of these deep roots remains contentious. Cratons produce over 90% of the world's gold and platinum and almost 100% of its diamonds. The properties of cratonic lithospheric roots are becoming increasingly recognized as key factors in the topographical expression of continents[3], lithospheric volatile storage[4] and the location of many metal deposits[5].

Understanding the role of lithospheric mantle in the stabilization and subsequent protection of continents requires clarification of the term craton. The original use - kratogen - from the Greek "kratos" meaning strong[6], merely implied a continental terrane displaying long-term stability of 100s of Myr, with no age definition. Following Kennedy[7], Clifford[8] recognized an association of ancient continental masses (> 1.5 Ga) with certain mineral deposits, especially diamonds, gold and platinum, though more recent widespread use of "craton" has become synonymous with Archean regions. Yet many "cratons" have long-lived tectonic histories that belie the image of post-Archean "stability".

Studies of the Kaapvaal craton (**Box. 1**), generally use a craton definition specifying a region where basement crustal rocks are > 2.5 Ga (e.g., [9]) yet major mid-craton disruption and magmatic addition affected it in Paleo- and Mesoproterozoic times. Studies of the Siberian and Amazonian cratons (**Fig. 1**) have followed the broader definition[10] of "a segment of continental crust that has attained and maintained long-term stability, with tectonic reworking being confined to its margins". For the 4.1 million km^2 Siberian craton, much of the crust surrounding two Archean nuclei was either intensely metamorphosed or formed in Paleoproterozoic times[11]. Similarly, the Amazonian craton has only a small area of clearly established Archean crust[12] within large regions of Paleoproterozoic crust[13]. It, along with numerous other cratons (e.g., Rae, Hearne & Gawler; **Fig. 1**) have been extensively intruded by felsic plutons in the Paleo- and Mesoproterozoic making the restriction of the definition of a craton to geological inactivity since the Archean problematic.

A thick lithospheric mantle has long been identified as a distinguishing feature of cratons, intimately linked to their stability (e.g., [2,14 15 16 17]). Hence, it seems logical to involve the mantle root in the definition of a craton. These deep strong mantle keels play a role in protecting the overlying crust from subsequent reworking and recycling, diverting mantle plume heat and mass fluxes away from the roots[18] without significant modification, unless weakened by metasomatism[19,20].

Seismology can be used to assess the correlation between deep cratonic mantle roots and ancient crust (**Fig. 1**). Areas underlain by cool, thick (>150 km) lithospheric mantle roots with anomalously fast seismic wave speeds extend well beyond the ~55 Archean nuclei of continents[21-25] (**Box 1; Fig. 1**), underpinning the much larger projected outlines of composite terranes amalgamated and stabilised in the Paleo- to Mesoproterozoic, for instance well into the Mesoproterozoic terranes of North America[24]. It is clear from seismology and geochronology (**Fig. 1; Box 1&3**) that the thickest lithosphere is not exclusive to the oldest crust, and most of Earth's crust older than ~ 1 Ga has >150km thick lithospheric roots[26] that have been present since that time[16]. This naturally leads to a more practical definition of craton:

Cratons - *are coherent blocks of Precambrian lithosphere, typically stable for time periods in excess of a billion years due to protection by deep (> 150km) lithospheric keels. The majority of Earth's Archean crust lies within such terranes and can be referred to as Archean cratons or nuclei. But the moniker "craton" is not exclusive to the Archean. Larger composite cratons may consist of Archean nuclei surrounded by Palaeo- Mesoproterozoic crust, all underpinned by thick cool lithospheric mantle. Supercratons comprise multiple composite cratons (Fig. 1).*

Cluster analysis of seismic tomographic models[23] or lithospheric thermal properties[27], can produce regionalized maps of upper mantle structure by identifying similar types of lithospheric mantle. These maps (e.g., Supplementary **Fig. 1)** successfully match thick lithosphere with the above definition of cratons, significantly increasing the contiguous cratonic area of some regions such as the southern African supercraton[26] and in global terms (**Fig.1**). Cratons, as defined here, comprise ~ 63% of the exposed continental surface, or ~ 18% of Earth's surface [Supplementary **Fig. 1**].

Exceptions are areas of Archean crust that have recently lost an old thick lithospheric keel and are now underlain by relatively thin (<100 km) lithosphere, e.g., the eastern North China and Wyoming cratons (**Fig. 1**). Crust in these regions survived for billions of years likely because they were protected by a thick root until lithosphere thinning in Phanerozoic time[28,29,30,31]. They are classified as "modified cratons". Regions of young crust, underlain by thick lithosphere such as Tibet, or the Central Asian Orogenic Belt (**Fig. 1**) have not yet achieved cratonic stability, but may do so[26].

2.2 Cratonic mantle lithosphere – composition and properties

Earth's upper mantle, based on sampling, theory and experiment, is composed largely of peridotite[32], typically a rock dominated by olivine, along with orthopyroxene, clinopyroxene and an Al-rich mineral that, depending on pressure and bulk composition, is garnet or spinel beneath continents [**Box 1a**], or rarely plagioclase (<1 GPa). Extraction of melt from peridotite is the key process defining the formation of Earth's lithospheric mantle. Mantle peridotites residual after significant melt extraction are referred to as "depleted" whereas compositions similar to estimates of un-melted mantle are known as "fertile" (**Box 2**).

Fertile mantle is characterized by the peridotite sub-type lherzolite, which transforms to harzburgite then dunite as clinopyroxene and then orthopyroxene are consumed by progressive melting (**Box 2**). The shift from fertile to depleted compositions has a major influence on peridotite density since Fe is preferentially extracted over the atomically lighter Mg from olivine, the main mantle mineral. In addition, Al - a key component of the dense minerals garnet and spinel - is removed in the melt[14]. A maximum of ~ 2.5 % reduction in bulk density occurs from fertile lherzolite to ultra-depleted dunite [33] (**Box 2**). The resulting systematic variations in Fe and Mg and, in turn, the degree of depletion can be traced via the Mg# (molar 100*Mg/[Mg+Fe]) of olivine, which depends on the upwelling path of the mantle during melt extraction as well as the efficiency of melt removal[33-39]. Different melting paths engender differences of ~ 0.62% in density at 35% melt extraction[33] (**Box 2**).

Compositionally-derived density decrease combined with the higher viscosity of cooler melt-depleted lithospheric mantle imparts physical stability to continental lithosphere [2,14]. Also, water - as dissolved hydrogen - is a primary control on mantle viscosity[40]. Melt-depleted, dry, cool lithospheric mantle is much more viscous, and hence stronger, than fertile, warmer upper mantle that has higher water contents, with viscosity and buoyancy being key to the robustness of continental roots [41,42] against attack by tectonic processes and mantle plumes.

Seismic[22,24-26] and gravity data[43] indicate that cratonic lithosphere is heterogeneous and that the lithospheric mantle sampled by deeply-derived melts such as kimberlites (Mg-CO_2 H_2O-rich low-volume magmas) may be compositionally atypical, showing more extensive effects from re-fertilisation due to melt/fluid infiltration (metasomatism). For instance, tens of km-scale seismic heterogeneities beneath the Lac de Gras kimberlite field, Canada[44], likely represent mantle modification by intruded kimberlites. Also, most lithospheric sections sampled as xenoliths/xenocrysts indicate that the lowermost lithosphere in regions of kimberlite activity is more Ti and Fe-rich than mantle overlying it[45,46] due to metasomatism.

Geophysical observations of cratonic mantle and the lack of kimberlite eruptions in the thickest lithosphere[26] imply that the mantle peridotite xenolith record may provide a biased view – as recognised by petrologists[47]. Modified compositions and mineralogies in many xenoliths are recorded by anomalously high clinopyroxene and/or garnet contents relative to their very elevated Mg#[48,49] and trace element systematics of clinopyroxene and garnet that commonly reflect their formation from, or equilibration with migrating fluids or melts long after lithosphere formation[50-53].

Despite the modified nature of many cratonic mantle xenoliths, no other samples exist. Petrological approaches to correct for the effects of metasomatism can infer the nature of the unmodified peridotite protolith[54-56]. Compositions derived from these approaches agree with the compositions of the most depleted, least modally metasomatized cratonic peridotite suites, e.g., Murowa, Zimbabwe craton[57]; East and West Greenland[34,48,58,59] i.e., that much of the cratonic mantle lithosphere, away from effects of kimberlite transit, comprises harzburgites or dunites with high Mg but low Ca and Al .

2.3 Melting conditions

How do such depleted peridotite compositions originate? The suggested tectonic melting regimes vary from deeply-derived mantle plumes (high average pressure of melting: > 5 GPa) building lithosphere by vertical accretion of residues[55,56,60,61] to decompression melting in rift-related environments (low average pressure of melting: < 5 GPa), beneath thin lithosphere, for instance at mid-ocean ridges[47,62-72], or hydrous flux-melting in the mantle wedges of subduction zones[73-76].

The different genetic hypotheses have been supported by different geochemical arguments. Authors favoring high-pressure (> 5 GPa) mantle plume melting highlight the low FeO of many Archean peridotites as indicating melt extraction at 5 to 7 GPa[55,56,77,78]. However, the spread in FeO contents is large, elevated by some types of melt metasomatism and lowered by orthopyroxene growth from Si-rich melts/fluids[67,79]. While deep-plume initiated polybaric melting beginning at high pressures and ending at low pressures beneath thin lithosphere is most effective in extracting the highest total melt-fraction from peridotitic mantle [**Box 2**], melting initiated at lower pressures, under rifts or hot spreading centres, where melting might begin at 5 GPa due to elevated mantle potential temperatures in the Archean and Paleoproterozoic[66,67,70,80] is also effective at removing melt fractions of between 30 to 40 %. Such melt fractions can generate the typical olivine Mg#s of cratonic peridotites[37,66] and reproduce olivine Mg# versus depth trends[81]. More definitive is the systematic variation in heavy rare earth element (HREE)[62,67,71,72,76,82] (**Fig. 2**) and transition metal element concentrations[63] indicating that garnet was not a residual phase during most of the melting regime, that began at 5 to 3 GPa.

Mineral chemistry is also a powerful indicator of the depth of melting. High-Cr garnets in cratonic peridotites and peridotite-type diamond inclusions are best explained by high-pressure metamorphism of melt residues that originally formed at lower pressures, in the spinel stability field[71]. The range of high-temperature garnet compositions produced in experimental melt-residues or via exsolution from high-pressure melting residues is narrow and low in Cr (3 - 5 wt % Cr_2O_3), contrasting strongly with the extended range to higher Cr contents in cratonic peridotite garnets. The higher garnet Cr contents are generated by metamorphic formation of garnet - at high pressures - from melt residues produced as spinel peridotites during melting at lower pressures[62] [83]. Some cratonic garnet may have exsolved from high-T orthopyroxene, but calculated pre-exsolution host orthopyroxene compositions have high Al and low Ca, likely formed in shallow melting residues within the spinel stability field[84].

Some have suggested, from bulk rock chemistry, that the parental low-pressure melt residues may have been serpentinites[85,86] or that parts of the keel formed from hydrous diapirs from hydrated slabs in the transition zone[87]. However, oxygen isotope compositions in cratonic peridotites are remarkably homogenous and "mantle-like", over a wide range of Cr and Si contents[88] precluding a serpentinite or hydrated slab origin.

High-pressure, plume-derived melt residues, produced through Earth history, may also be present in cratonic lithosphere because they too are buoyant and viscous and may be entrained during lithosphere accretion. In one conspicuous case, cratonic lithosphere of the north Slave craton has been thinned by plume erosion and re-thickened [89] by the trapping of higher-pressure melting residues in the "thin-spot", as traced by geochemistry (**Fig. 2**).

However, while such residues contribute to the compositional heterogeneity of cratonic mantle, their contribution, based on the geochemical evidence, appears to be subordinate, with the combined trace-element and mineralogical evidence dominantly reflecting a lower pressure (< 5 GPa) polybaric decompression melting regime. That many cratonic peridotites now record equilibration pressures > 5 GPa requires tectonic transport of these buoyant shallow-formed melting residues to greater depth during thickening of the lithospheric roots during craton-formation processes[62,65,66,71,72,74-76,83,90].

2.4. Age structure of cratonic mantle, crust-mantle relations and temporal trends

Having established the presence of widespread thick mantle lithosphere beneath continental crust of Archean through Mesoproterozoic age (**Fig. 1; Box 1**) as a key ingredient of cratons, it is important to examine specific age relationships between cratonic roots and their overlying crust, which can constrain the mode craton formation. A challenge is that peridotite ages recorded by trace-element isotopes are not, in all cases, the age of formation of the lithospheric keels – a fact well illustrated by the very large spectra of melting ages for peridotites found beneath the very young continent of Zealandia[91] or the ancient Os model ages observed in abyssal peridotites[92,93].

Early radiogenic isotope studies of cratonic mantle and inclusions in diamonds showed very different isotopic signatures to the asthenosphere, establishing isolation of lithospheric mantle for Gyr periods[94-96]. The Rb-Sr, Sm-Nd and U-Pb systems used in these studies have very low parent-daughter element concentrations in residual peridotite relative to mantle melts. Hence the ages dominantly reflect "enrichment ages" due to metasomatism rather than the age of the melt extraction relating to lithosphere formation. Subsequent application of the ^{187}Re-^{188}Os decay system to mantle peridotites produced ages that more likely reflected the approximate age of melt depletion[29,61,77,97] [**Box 3**].

Widespread application of the Re-Os isotope system to dating lithospheric peridotites has led to a clearer picture of the age of cratonic mantle roots, though the approach is a blunt tool in terms of providing a precise estimate of when melt depletion occurred[76,81,98-103]. Critically, because Os isotope heterogeneity in Earth's mantle increases with time, interpretation of Re-Os model ages from peridotites or sulfides younger than ~ 1.5 Ga have large uncertainty because of the isotopic diversity of Phanerozoic mantle [**Box 3**]. Portions of modern oceanic lithospheric mantle frequently produce Re-Os model ages of over 1 Ga and sometimes up to 2 Ga, at the mineral to meter scale[92,93]. This heterogeneous "age" spectrum for modern mantle lithosphere demands caution when interpreting single occurrences of ancient ages of 1 to 2 Ga in a lithospheric peridotite suite dominated by much younger ages, derived from Os isotope compositions that are statistically identical to modern upper mantle. Instead, some studies infer the ubiquitous presence of Archean mantle, refertilised in Proterozoic or younger times, from the occurrence of a single Archean Re-Os model age in a peridotite suite[104]. But it is increasingly clear that mantle peridotite age spectra are strongly influenced by the persistence of ancient ages in the upper mantle[105,106]. Similarly, while more ancient Os model ages can be sometimes recovered from sulfide or alloy grains in peridotites than from most whole-rock analyses in a given suite[93,103,107-109], it is important to better understand the spectrum of Os isotope heterogeneity in Archean mantle before interpreting isolated older ages as the age of lithosphere formation, even though these estimates may well prove accurate with extended studies.

With the above context, we can now explore questions such as: What are the oldest components of cratonic lithospheric mantle and what is the likely age of formation / stabilization of the lithospheric keels? Six first-order observations are:

1) Some cratons contain crust of Hadean or Eoarchean age, but no such ages are preserved for cratonic mantle, precluding a primary origin for cratonic roots as lithosphere formed, for instance, during any early "stagnant lid" phase of Earth's evolution e.g.[110]. Some melting residues from these times may have been incorporated into cratonic roots, their ages over-printed.

2) Though mantle melt residues were clearly being produced by Earth before the Mesoarchean, the vast majority of the peridotite depletion ages are Meso- to Neoarchean, documenting the rapid growth of thick cratonic keels over a shorter period, and at a different rate than the continental growth curve (**Box 3**).

3) A peak in depletion ages between 2.0 and 1.8 Ga occurs in mantle lithosphere beneath Archean and Proterozoic cratons (**Box 3**), indicating mantle root formation in the Paleoproterozoic[111-114], either coincident with the assembly of some larger composite cratons e.g., Siberia, or prior to / during the formation of the Nuna supercontinent, which created some of the larger composite cratons observed today.

4) Despite the association of predominantly Archean mantle underlying Archean nuclei and Proterozoic mantle underlying Proterozoic cratons (Box 3), more age decoupling exists between crust and mantle than originally proposed, e.g.,[77], with lithospheric mantle recording Archean melt extraction underlying Paleoproterozoic crust[48,115], Paleoproterozoic mantle residues underlying Archean crust[114], Neoarchean mantle residues underlying Meso- to Eoarchean crust[116] and Mesoproterozoic residues underlying Neoarchean crust[89].

5) Archean melt residues form some of the lithospheric building blocks to Proterozoic cratons. Vestiges of these foundations are also seen in lithosphere beneath modified cratons, but these lithospheric sections have been mostly replaced by more recent mantle (**Box 3**)

6) With the exception of Tibet or the Central Asian Orogenic Belt - cratons in the making[26] - lithospheric mantle underlying regions of thick (>150km) continental lithosphere formed > 1 Ga ago **(Box 1; Fig. 1)** .

These points are amplified in the context of specific cratons. The Kalahari composite craton, lying within the southern African supercraton, comprises the Kaapvaal and Zimbabwe Archean nuclei and associated Proterozoic terranes (**Box 1b**). The nuclei show broad age correspondence between Archean crust and highly depleted Meso- to Neoarchean cratonic mantle[62,74,76,77,82,98,100,109,117]. Where younger lithosphere ages exist, such as the center of the Kaapvaal nucleus (Premier kimberlite) the Paleoproterozoic melt depletion ages (**Box 1b**)[74,77] reflect major rifting, disruption and healing of the craton at ~ 2 Ga, coincident with the formation of the massive Bushveld complex. The overall crust-mantle age relations indicate a diachronous Meso- to Neoarchean stabilisation age for the ~ 200 km thick lithosphere across the Archean nucleus (**Box 1b**)[118], reflected by the broad mode of peridotite Re-Os model ages. In the outer portions of the Kalahari craton, crust in the Rehoboth and Namaqua-Natal terranes is ~ 1.3 to 2.2 Ga[119] (**Box 1b**). Peridotite xenoliths indicate the roots beneath these outer cratonic regions are up to 200 km thick and Re-depletion ages range from 1.2 to 2.4 Ga (single locality modes between 1.25 and 1.75 Ga [120]) potentially reflecting lithospheric mantle produced during pulses of juvenile magmatism[121]. Subsequent accretion to the craton during the Namaqua-Natal accretionary orogen created the thick lithosphere observed beneath most of this Proterozoic cratonic region imaged by seismology[22,25,122] (**Fig. 1**).

The high degree of crust-mantle age "coupling" beneath cratons implied by early work[16,77] has not withstood further scrutiny (**Box 3b**). For instance, in the Siberian craton, Re-Os and Lu-Hf dating shows that while some remnant Archean mantle is present, the dominant melt depletion event for cratonic peridotites beneath the Daldyn-Markha portion of the Anabar Archean nucleus occurred ~ 2.0 to 1.8 Ga[111,112,123], whereas highly-depleted lithospheric mantle beneath the Olenek terrance of the same nucleus is predominantly Archean[123,124]. A complex age structure is also evident in the mantle beneath the central Rae craton, northern Canada, where older, shallow Archean mantle is underlain by mantle that either formed, or was massively over-printed at circa 1.8 Ga[125]. Similarly, the Archean Sask craton (Canada) is underlain by mantle depleted at ~ 1.8 to 2 Ga, associated with the Trans-Hudson orogeny[114], and the central Superior craton experienced significant lithosphere replacement during the Mesoproterozoic [126]. In contrast, the Paleoproterozoic Halls Creek orogen (West Australia composite craton) is underlain by deep lithospheric mantle of Archean age[115], and a similar relationship exists in East[48] and West[116] Greenland, part of the Laurentia supercraton (**Fig. 1**).

Some Paleoproterzoic cratonic peridotites have highly depleted major-element and mineral compositions resembling those formed in the Archean, e.g., in Arctic Canada[113] (**Box. 1a).**

This and other examples[58,67,91,127] indicate that very depleted melt residues can be produced well beyond the Archean/Proterozoic boundary, in contrast to some proposals[55,128]. Such highly depleted Paleoproterozoic lithospheric mantle became incorporated into craton roots during major post-Archean craton-forming accretionary orogens[129].

The variation in peridotite compositions - and hence melting conditions - with geological time is of interest in understanding the origins of cratonic peridotites as well as mantle thermal evolution[70,80,130]. A recent approach[70], augmented here using the most reliable estimates of melting ages for peridotite suites screened via criteria such as extended PGE patterns[81,103] (**Box 3b)** indicates that the apparent secular decrease in peridotite olivine Mg# with decreasing model age (excluding Phanerozoic arc peridotites) fits well with the expected trend of secular decrease in mantle potential temperature, at Urey ratios of between 0.2 and 0.3. This fit, though imperfect, suggests that no anomalously hot mantle plume is required to explain the melting regime of cratonic peridotite residues, consistent with an origin via relatively shallow decompression melting[70].

2.5 Formation of cratons and cratonic mantle – the importance of lateral accretion

In the context of craton formation, the debate over the relative roles of residual peridotites formed by mantle plume melting versus those formed by the thickening of residues of shallow polybaric decompression melting can be addressed through geodynamic modelling. Mantle lithosphere above modern mantle plumes experiences net lithospheric thinning, e.g., beneath Hawaii, where the maximum lithosphere thickness is equal to or thinner than normal oceanic lithosphere[131]. Similarly, in the central North Atlantic craton, the ~ 200 km thick mantle root present throughout the Proterozoic Eon[132,133] was thinned locally to 60 km by ~ 60 Ma plume activity[134]. The Ontong Java plateau is an exception since mantle xenoliths reveal a lithosphere exceeding 120 km[135]. but the uppermost 80 km formed from normal oceanic lithosphere[136]. Beneath Africa, seismology indicates that plumes are the sites of lithosphere erosion[137] and are implicated in plate destruction, not growth[138].

Geodynamic modelling of the dispersion of plume melting residues (**Fig. 3; Supplementary Video 1**), shows that excess mantle potential temperatures in the upwelling plume, in an ambient mantle that was ~200 K hotter than the present-day MORB source are sufficient to counteract viscosity increases due to melt depletion, allowing rapid dispersal by the plume mass flux, either back into the upper mantle or forming relatively thin, widespread layers of residual mantle, adding slightly to lithospheric depth but not attaining the 200 km thickness of most cratonic lithosphere. Compressional thickening is required to achieve cratonic root thicknesses. Buoyant plume residues seem to be effective at "re-cratonising" lithosphere, after plume-related thinning, coalescing to re-form > 150 km thick lithosphere[89]. In contrast, the residues of high degrees of decompression melting at low average pressures, in rift environments remain at their sites of generation. These residues form at lower mantle potential temperatures, cooling more rapidly to attain the high viscosities needed for stabilization of cratonic roots[3,139]. The lithospheric columns produced by such melting must then be thickened to depths seen in cratonic roots.

The dominant lithosphere during Archean times was unlikely to have been as dynamic as in modern-day ocean basins, with perhaps only episodic mobility and nascent subduction-like features[139,140]. Hence, while extensive polybaric decompression melting at low average pressure is required by cratonic peridotite geochemistry, long-lived mid-ocean ridge spreading centres may not have been as extensive in the Archean as in modern Earth. Other models of early Earth lithosphere dynamics invoke extensive melt extraction at sites of lithosphere rifting/divergence leading to formation of segments of strong buoyant lithospheric “blocks” via strain localization and cooling, sustaining further extension and melting[139] . The resulting mix of depleted lithospheric blocks can amalgamate and thicken via lateral compression/accretion and further cooling into ~ 200 km thick, depleted, cool, cratonic lithospheric roots[141].

Lateral accretion, by either compression during the formation of accretionary orogens or a shallow subduction-like processes involving slab stacking, has long been invoked to play a role in the thickening and stabilization of old and young continental masses and their lithospheric roots[14,67,91,142-145] and has been illuminated by recent geodynamic simulations[141,146]. Starting with even present-day thicknesses of melt-depleted oceanic lithosphere, lateral compression, perhaps driven by the initiation of some form of subduction, can generate stable 200 km-thick mantle keels via tectonic and gravitational thickening associated with cooling (**Fig. 3**). This requires the pre-existence of a strong and buoyant depleted mantle lithosphere, such as that produced at rifted margins or spreading axes, which, along with the crust, thickens by compression.

What is the evidence for lateral accretion and compressive thickening? Plate-scale deformation imparts anisotropic fabrics on lithospheric peridotite through lattice-preferred orientation of olivine, detectable with seismology[147]. Seismic anisotropy typically occurs in the upper 150 km of most cratonic lithospheres and is usually interpreted as a deformation fabric created during the formation and evolution of the craton structure[148]. A change in the seismically fast axis of olivine, from horizontal at depths < 150 km to vertical at depths > 150 km in cratonic roots[149] has also been proposed as evidence for lithospheric shortening via compression in making the deep roots to cratons.

The geological evidence for lateral accretion and compression during craton assembly is equally compelling. Most cratonic crust is constructed from numerous individual "blocks" or terranes, now juxtaposed with relatively high aspect ratios, e.g., the Superior craton. Such complex large-scale linear geological fabric requires either subduction or some other lateral accretion process during assembly in accretionary orogens to construct the final craton, perhaps over multiple cycles [129,150,151]. In some cratons, e.g., Pilbara, these relationships are not as clear, though most comprise different blocks/terranes that were not originally contiguous. Thrust-bounded terranes characterize the assembly of the Neoarchean potions of cratons[17,129], with large-scale continental thrust structures observed back into the Mesoarchean[152], clearly documenting compression of lithosphere. Compression and thickening of lithosphere have thermal consequences for the crust[153,154] and offer a mechanism - via consequent crustal melting - to produce the prominent post-orogenic granitic magmatism, sourced in-part or wholly by crustal melting, especially when heat-producing nuclides were more abundant in the Archean. Such post-orogenic magmatism, often of a potassic nature, is widespread in cratons, e.g., 2.61 to 2.58 Ga granites of the Slave craton[155]; 3.1 Ga granites of the Kaapvaal craton[121]; 2.67 - 2.62 Ga post-orogenic granites of the Superior craton[151]; 2.6 Ga Snow Island granites of the Rae craton[156], and is incompatible with a low geothermal gradient in the lower crust that would be expected from the presence of already stable thick, cool cratonic mantle roots. High-T granulite-facies metamorphism accompanies such lithospheric thickening and is among the hallmarks of "cratonisation" of the crust. In the Proterozoic, craton assembly continued via lateral accretion during compressive orogens, as is clearly illustrated by the evolution of the Laurentia supercraton [148,150,157] , producing striking widespread radial seismic anisotropy in the lower craton root[149], and the Siberian composite craton, where 1.8 Ga granulite-facies metamorphism is widespread.

These features of cratons and their roots illustrate that whatever the various models invoked for the genesis of their crust and mantle components, the decisive final phase of assembling and stabilizing cratons, from the Archean through to the Mesoproterozoic, is lateral accretion, compression and lithospheric thickening, as originally envisioned by Jordan [14]. It should be no surprise that the thickest parts of Earth's lithosphere on the modern Earth, outside the cratons are in zones of continental convergence[158], [144].

3. Broader implications and directions

Through the Archean, the relationship between peridotite melt-depletion ages, which broadly track the melting that formed the cratonic roots, and the continental growth curve [**Box 3**] indicates a disconnect in the genesis of the continental crust and underlying mantle root. Continental crust genesis began much earlier, growing through a longer time interval, at a different rate. Since the end of the Archean, the cratonic mantle depletion curve and the continental growth curve are mirror images. Assembly and stabilization of thick, viscous cratonic roots were critical to the preservation of Earth's continents. This is supported from the first appearance, ~2.8 Ga, of mature sediments in the stratigraphic record, with great diversity in zircon ages [**Box 3**], likely tracking the first significant rise of continents above sea level[159] due to the stabilisation of protective cratonic mantle roots in the Meso- to Neoarchean.

Cratonic root formation continued to take place through the Proterozoic but the genesis of highly melt-depleted peridotites that formed the craton roots waned significantly after 1 Ga (**Box 3**), perhaps due to mantle cooling. However, mantle residues produced in some Phanerozoic oceanic arcs are as depleted as cratonic peridotites (**Box 3**). Future cratons may be underpinned by the depleted residues of arc melting, swept up during continental assembly, for example, during the formation of Earth's newest continent, Zealandia, a 4.9 million km^2 block of continental crust created in Pacific arc settings and underlain by locally very depleted lithospheric mantle[91] extending over 150km deep where collisional thickening is greatest[160]. Understanding these recently-formed continental masses and their collisional roots will be key to understanding how thick lithosphere grows, stabilizes and evolves. If the majority of cratonic lithosphere is more depleted than the peridotite record, mantle roots will be more buoyant, affecting hypsometry.

Defining what cratons are, and how their lithosphere evolves is critical to finding mineral deposits. For instance, the spatial association between base metal deposits and the transition between thick and thin lithosphere provides a basis for further exploration[5].

Our definition of cratons as stable regions of ancient crust, protected by ≥ 150 km thick lithospheric mantle roots, which have experienced minimal tectono-magmatic disturbance since the end of the Mesoproterozoic (1 Ga), (**Box 1, Fig. 1**) is clearly a pragmatic generalization. It is clear that cratons and their roots are periodically disrupted by rifting and invaded by magmatic products. It is also evident that some cratons lose part of their mantle root through disruption and weakening and then may "re-cratonise"[89], re-establishing thick lithosphere and long-term stability. This re-healing process contributes to the patchwork of lithosphere observed and also is associated, in some cases, with world-class mineral deposits, such as the Bushveld intrusion or Premier/Cullinan diamond mine. Understanding what controls the extent of these craton-disrupting events and how they localize mineralization is important for mineral exploration.

More fundamentally, searching for evidence of a role for Hadean /Eoarchean melting residues in the evolution of lithospheric mantle will help understand the fate of Earth's earliest lithosphere, possibly produced in a stagnant lid tectonic regime, but conspicuously absent from the rock record. These early melting residues may have been quickly recycled back into the upper mantle because too rapid compression/accretion of lithosphere and insufficient depletion-related strengthening prevented deep lithospheric roots from stablising[139,141]. What remain now as the long-lived lithospheric roots to continents are the successful attempts to stabilize these masses. While evidence of very early melt residues remains elusive, the increasing occurrence, within young lithosphere of oceanic[92,105,106] and continental[91] affinity, of peridotites or mantle minerals with Archean melt-depletion ages may represent the "ghosts of lithospheres past", recycled back into the upper mantle and re-housed in later lithosphere construction. Understanding what these vestigial ages tell us about how lithosphere is destroyed and re-constructed, billions of years apart, should be a future endeavor for geochemists.

The links between hypsometry, continental crust and its underlying lithosphere require further scrutiny. The coincidence between a change in continental freeboard towards presents levels by Meso- to Neoarchean times, reflecting the emergence of major continental masses, and the establishment of thick cratonic roots is striking (Box 3)[159]. This implicates a central role for newly formed, stable continental masses – cratons – with special attributes, i.e., thick crust comprising a strong lower crust that is dehydrated and depleted of its heat producing elements by thickening-induced melting or granulite facies metamorphism. How these or other attributes were able to offset any negative thermal buoyancy imparted by the thick cratonic mantle roots underlying this crust requires further clarification. Such cratonic lithosphere, for the first time, appears to have been able to support orography similar to that of modern continents.

REFERENCES

1 Artemieva, I. M. *The Lithosphere: An interdisciplinary approach*. 794 (Cambridge University Press, 2011).

2 Jordan, T. H. Continental tectosphere. *Reviews of Geophysics* **13**, 1-12, doi:10.1029/RG013i003p00001 (1975).
Key to recognising the fast seismic wave speeds and deep thermal boundary layers beneath parts of the continents. Recognised the need for compositional compensation of the negatve thermsl buoyancy of continental lithosphere

3 Eaton, D. W. & Claire Perry, H. K. Ephemeral isopycnicity of cratonic mantle keels. *Nature Geoscience* **6**, 967-970, doi:10.1038/ngeo1950 (2013).

4 Gibson, S. A., Rooks, E. E., Day, J. A., Petrone, C. M. & Leat, P. T. The role of sub-continental mantle as both “sink” and “source” in deep Earth volatile cycles. *Geochimica et Cosmochimica Acta* (2020).

5 Hoggard, M. A. *et al.* Global distribution of sediment-hosted metals controlled by craton edge stability. *Nature Geoscience* **13**, 504-510 (2020).

6 Kober, L. *Der Bau der Erde*. (Gebr¨ uder Borntraeger, 1921).

7 Kennedy, W. Q. The structural differentiation of Africa in the Pan-African (+/- 500 m.y.) tectonic episode. *Annual Report of the Research Institute of African Geology, University of Leeds*, 48-49 (1964).

Laid the foundations of recognising stability as a key part of continental evolution and mineralisation, inspiring Clifford - below.

8 Clifford, T. N. Tectono-metallogenetic units and metallogenetic provinces of Africa. *Earth and Planetary Science Letters* **1**, 421-434 (1966).

9 Dewit, M. J. & Hart, R. A. Earths Earliest Continental Lithosphere, Hydrothermal Flux and Crustal Recycling. *Lithos* **30**, 309-335 (1993).

10 Bleeker, W. Archaean tectonics: a review, with illustrations from the Slave craton. *Geological Society, London, Special Publications* **199**, 151-181 (2002).

11 Priyatkina, N., Khudoley, A. K., Collins, W. J., Kuznetsov, N. B. & Huang, H.-Q. Detrital zircon record of Meso- and Neoproterozoic sedimentary basins in northern part of the Siberian Craton: Characterizing buried crust of the basement. *Precambrian Research* **285**, 21-38, doi:10.1016/j.precamres.2016.09.003 (2016).

12 Santos, J. O. S. *et al.* Duration of the Trans-Amazonian Cycle and Its Correlation within South America Based on U-Pb SHRIMP Geochronology of the La Plata Craton, Uruguay. *International Geology Review* **45**, 27-48, doi:10.2747/0020-6814.45.1.27 (2003).

13 Carneiro, M. A., Júnior, I. M. D. C. & Teixeira, W. Petrologia, geoquímica e geocronologia dos diques máficos do complexo metamórfico bonfim setentrional (quadrilátero ferrífero) e suas implicações na evolução crustal do craton do São Francisco meridional. *Revista Brasileira de Geociências* **28**, 29-44 (2017).

14 Jordan, T. H. Composition and development of the continental tectosphere. *Nature* **274**, 544-548 (1978).

Furthered the notion of the compositionally induced robustness of continents to convective disruption and proposed a compressional thickening model for the origin of deep continental roots

15 Boyd, F. R. & Gurney, J. J. Diamonds and the African Lithosphere. *Science* **232**, 472-477 (1986).

16 Pearson, D. G. The age of continental roots. *Lithos* **48**, 171-194 (1999).

17 Hawkesworth, C. J., Cawood, P. A., Dhuime, B. & Kemp, T. I. S. Earth's Continental Lithosphere Through Time. *Annual Review of Earth and Planetary Sciences* **45**, 169-198, doi:10.1146/annurev-earth-063016-020525 (2017).

18 Sleep, N. H., Ebinger, C. J. & Kendall, J. M. Vol. 199 135-150 (Geological Society, London, Special Publications, 2003).

19 Foley, S. F. Rejuvenation and erosion of the cratonic lithosphere. *Nature Geoscience* **1**, 503-510, doi:10.1038/ngeo261 (2008).

20 Wang, H., van Hunen, J. & Pearson, D. G. The thinning of subcontinental lithosphere: the roles of plume impact and metasomatic weakening. . *Geochemistry, Geophysics, Geosystems* **16**, 1156-1171 (2015).

21 Simons, F. J., Zielhuis, A. & van der Hilst, R. D. The deep structure of the Australian continent from surface wave tomography. *Lithos* **48**, 17-43, doi:10.1016/s0024-4937(99)00041-9 (1999).

Showed the widespread presnce of very deep mantle roots beneath western Australia, outside of Archean nuclei.

22 James, D. E., Fouch, M. J., VanDecar, J. C., van der Lee, S. & Kaapvaal-Seismic-Group. Tectospheric structure beneath Southern Africa. *Geophysical Research Letters* **28**, 2485-2488 (2001).

23 Schaeffer, A. & Lebedev, S. in *The Earth's heterogeneous mantle* 3-46 (Springer, 2015).

24 Schaeffer, A. J. & Lebedev, S. Imaging the North American continent using waveform inversion of global and USArray data. *Earth and Planetary Science Letters* **402**, 26-41, doi:10.1016/j.epsl.2014.05.014 (2014).

25 Ortiz, K. *et al.* Upper mantle P and S wave velocity structure of the Kalahari Craton and surrounding Proterozoic terranes, southern Africa. *Geophysical research letters* **46**, 9509-9518 (2019).

26 Mckenzie, D. & Priestley, K. The influence of lithospheric thickness variations on continental evolution. *Lithos* **102**, 1-11, doi:10.1016/j.lithos.2007.05.005 (2008).

27 Artemieva, I. M. Global 1 degrees x 1 degrees thermal model TC1 for the continental lithosphere: Implications for lithosphere secular evolution. *Tectonophysics* **416**, 245-277, doi:DOI 10.1016/j.tecto.2005.11.022 (2006).

28 Menzies, M. A., Fan, W.-M. & Zhang, M. Paleozoic and Cenozoic lithoprobes and the loss of >120 km of Archean lithosphere, Sino-Korean craton, China. *In: H.M. Prichard, H.M. Alabaster, T. Harris and C.R. Neary (Editors), Magmatic Processes and Plate Tectonics.* Geological Soc., London, 71-81 (1993).

First to propose the dramatic lithospheric thinning beneath the eastern North China Craton

29 Carlson, R. W. & Irving, A. J. Depletion and Enrichment History of Subcontinental Lithospheric Mantle - an Os, Sr, Nd and Pb Isotopic Study of Ultramafic Xenoliths from the Northwestern Wyoming Craton. *Earth and Planetary Science Letters* **126**, 457-472 (1994).

30 Gao, S., Rudnick, R. L., Carlson, R. W., McDonough, W. F. & Liu, Y. S. Re-Os evidence for replacement of ancient mantle lithosphere beneath the North China craton. *Earth and Planetary Science Letters* **198**, 307-322, doi:Pii S0012-821x(02)00489-2 (2002).

Convincing demonstration, using peridotite dating, of the ancient deep root of the North China Craton being replaced by shallow young lithosphere

31 Snyder, D. B., Humphreys, E. & Pearson, D. G. Construction and destruction of some North American cratons. *Tectonophysics* **694**, 464-485, doi:https://doi.org/10.1016/j.tecto.2016.11.032 (2017).

32 Ringwood, A. E. *Composition and petrology of the earth's upper mantle*. McGraw-Hill, (1975).

33 Afonso, J. C. & Schutt, D. L. The effects of polybaric partial melting on density and seismic velocities of mantle restites. *Lithos* **134**, 289-303 (2012).

34 Bernstein, S., Kelemen, P. B. & Brooks, C. K. Highly depleted spinel harzburgite xenoliths in Tertiary dikes from East Greenland. *Earth and Planetary Science Letters* **154**, 221-235 (1998).

35 Walter, M. J. Melting of garnet peridotite and the origin of komatiite and depleted lithosphere. *Journal of Petrology* **39**, 29-60 (1998).

Benchmark melting experiments that calibrate much of our understanding of how the composition of mantle melt residues vary with melt fraction

36 Herzberg, C. Geodynamic Information in Peridotite Petrology. *Journal of Petrology* **45**, 2507-2530, doi:10.1093/petrology/egh039 (2004).

37 Bernstein, S., Kelemen, P. B. & Hanghøj, K. Consistent olivine Mg# in cratonic mantle reflects Archean mantle melting to the exhaustion of orthopyroxene. *Geology* **35**, doi:10.1130/g23336a.1 (2007).

Recognised, using olivine composition, the ultra-depleted harzburgite/dunite nature of cratonic mantle, prior to ubiquitous metasomatism of these protoliths

38 Afonso, J. C. *et al.* 3-D multiobservable probabilistic inversion for the compositional and thermal structure of the lithosphere and upper mantle. I: a priori petrological information and geophysical observables. *Journal of Geophysical Research-Solid Earth* **118**, 2586-2617, doi:10.1002/jgrb.50124 (2013).

39 Baptiste, V. & Tommasi, A. Petrophysical constraints on the seismic properties of the Kaapvaal craton mantle root. *Solid Earth* **5**, 45 (2014).

40 Peslier, A. H., Schönbächler, M., Busemann, H. & Karato, S.-I. Water in the Earth's interior: Distribution and origin. *Space Sci Rev* **212**, 743-810 (2017).

41 Doin, M. P., Fleitout, L. & Christensen, U. Mantle convection and stability of depleted and undepleted continental lithosphere. *Journal of Geophysical Research-Solid Earth* **102**, 2771-2787, doi:Doi 10.1029/96jb03271 (1997).

Along with Lenardic (below) the pioneering dynamical models exploring the factors controling cratonic mantle root stability

42 Lenardic, A. & Moresi, L. N. Some thoughts on the stability of cratonic lithosphere: Effects of buoyancy and viscosity. *Journal of Geophysical Research: Solid Earth* **104 (B6)**, 12747-12758 (1999).

43 Artemieva, I. M., Thybo, H. & Cherepanova, Y. Isopycnicity of cratonic mantle restricted to kimberlite provinces. *Earth and Planetary Science Letters* **505**, 13-19, doi:10.1016/j.epsl.2018.09.034 (2019).

44 Snyder, D. B. & Lockhart, G. Does seismically anisotropic subcontinental mantle lithosphere require metasomatic wehrlite-pyroxenite dyke stockworks? *Lithos* **112**, 961-965, doi:10.1016/j.lithos.2009.03.033 (2009).

45 Smith, D., Griffin, W. L., Ryan, C. G. & Sie, S. H. Trace-Element Zonation in Garnets From the Thumb - Heating and Melt Infiltration Below the Colorado Plateau. *Contributions to Mineralogy and Petrology* **107**, 60-79 (1991).

46 Kopylova, M. G. & Russell, J. K. Chemical stratification of cratonic lithosphere: constraints from the Northern Slave craton, Canada. *Earth and Planetary Science Letters* **181**, 71-87, doi:10.1016/s0012-821x(00)00187-4 (2000).

47 Pearson, D. G. & Wittig, N. in *Treatise on Geochemistry (Second Edition)* (ed Heinrich D. HollandKarl K. Turekian) 255-292 (Elsevier, 2014).

48 Hanghoj, K., Kelemen, P., Bernstein, S., Blusztajn, J. & Frei, R. Osmium isotopes in the Wiedemann Fjord mantle xenoliths: A unique record of cratonic mantle formation by melt depletion in the Archaean. *Geochemistry Geophysics Geosystems* **2**, Paper number 2000GC000085, doi:2000gc000085 (2001).

49 Pearson, D. G., Irvine, G. J., Carlson, R. W., G., K. M. & Ionov, D. A. in *The Early Earth: Physical, Chemical and Biological Development* Vol. 199 65-90 (Geological Society, London, Special Publication, 2002).

50 Smith, D. & Boyd, F. R. Compositional Zonation in Garnets in Peridotite Xenoliths. *Contributions to Mineralogy and Petrology* **112**, 134-147 (1992).

51 van Achterbergh, E., Griffin, W. L. & Stiefenhofer, J. Metasomatism in mantle xenoliths from the Letlhakane kimberlites: estimation of element fluxes. *Contributions to Mineralogy and Petrology* **141**, 397-414 (2001).

52 Shimizu, N., Pokhilenko, N. P., Boyd, F. R. & Pearson, D. G. Geochemical characteristics of mantle xenoliths from Udachnaya kimberlite pipe. *Geologiya I Geofizika* **38**, 194-205 (1997).

53 Simon, N. S. C., Irvine, G. J., Davies, G. R., Pearson, D. G. & Carlson, R. W. The origin of garnet and clinopyroxene in "depleted" Kaapvaal peridotites. *Lithos* **71**, 289-322, doi:10.1016/s0024-4937(03)00118-x (2003).

54 Boyd, F. R. *et al.* Composition of the Siberian cratonic mantle: evidence from Udachnaya peridotite xenoliths. *Contributions to Mineralogy and Petrology* **128**, 228-246, doi:10.1007/s004100050305 (1997).

55 Griffin, W. L., O'Reilly, S. Y., Afonso, J. C. & Begg, G. C. The Composition and Evolution of Lithospheric Mantle: a Re-evaluation and its Tectonic Implications. *Journal of Petrology* **50**, 1185-1204, doi:10.1093/petrology/egn033 (2009).

56 Aulbach, S. Craton nucleation and formation of thick lithospheric roots. *Lithos* **149**, 16-30, doi:10.1016/j.lithos.2012.02.011 (2012).

57 Pearson, D. G. *et al.* in *Geoscience and Exploration of the Argyle, Bunder, Diavik and Murowa Diamond Deposits* Vol. 20 *Society of Economic Geologists Special Publication* (eds A.T. Davy *et al.*) Ch. 19, 403-424 (2018).

58 Bernstein, S., Hanghøj, K., Kelemen, P. B. & Brooks, C. K. Ultra-depleted, shallow cratonic mantle beneath West Greenland: dunitic xenoliths from Ubekendt Ejland. *Contributions to Mineralogy and Petrology* **152**, 335-347, doi:10.1007/s00410-006-0109-0 (2006).

59 Wittig, N. *et al.* Origin of cratonic lithospheric mantle roots: A geochemical study of peridotites from the North Atlantic Craton, West Greenland. *Earth and Planetary Science Letters* **274**, 24-33, doi:10.1016/j.epsl.2008.06.034 (2008).

60 Boyd, F. R. Compositional distinction between oceanic and cratonic lithosphere. *Earth and Planetary Science Letters* **96**, 15-26 (1989).
Documented the striking compositional contrast between modern oceanic and cratonic mantle lithosphere and proposed the latter are residues from komatiite extraction.

61 Pearson, D. G. *et al.* Re-Os, Sm-Nd, and Rb-Sr Isotope Evidence for Thick Archean Lithospheric Mantle beneath the Siberian Craton Modified by Multistage Metasomatism. *Geochimica et Cosmochimica Acta* **59**, 959-977 (1995).

62 Brey, G. P. & Shu, Q. The birth, growth and ageing of the Kaapvaal subcratonic mantle. *Mineralogy and Petrology* **112**, 23-41 (2018).

63 Canil, D. Mildly incompatible elements in peridotites and the origins of mantle lithosphere. *Lithos* **77**, 375-393, doi:10.1016/j.lithos.2004.04.014 (2004).

64 Gibson, S. A., Malarkey, J. & Day, J. A. Melt Depletion and Enrichment beneath the Western Kaapvaal Craton: Evidence from Finsch Peridotite Xenoliths. *Journal of Petrology* **49**, 1817-1852, doi:10.1093/petrology/egn048 (2008).

65 Helmstaedt, H. H. & Schulze, D. J. in *Kimberlites and related rocks. GSA Spec Publ 14* Vol. Vol. 1 (eds J. Ross & et_al.) 358-368 (Blackwell, 1989).

66 Herzberg, C. & Rudnick, R. Formation of cratonic lithosphere: An integrated thermal and petrological model. *Lithos* **149**, 4-15, doi:10.1016/j.lithos.2012.01.010 (2012).

67 Kelemen, P. B., Hart, S. R. & Bernstein, S. Silica enrichment in the continental upper mantle via melt/rock reaction. *Earth and Planetary Science Letters* **164**, 387-406, doi:10.1016/s0012-821x(98)00233-7 (1998).

First to outline a quantitative metasomatic origin for orthopyroxene enrichment in cratonic mantle - uses trace elements to document low-pressure melt extraction followed by higher pressure growth of metamorphic garnet

68 Lee, C.-T. A., Luffi, P. & Chin, E. J. Building and Destroying Continental Mantle. *Annual Review of Earth and Planetary Sciences* **39**, 59-90, doi:10.1146/annurev-earth-040610-133505 (2011).

69 Lee, C. T. A. in *Archean Geodynamics and Environments* 89-110 (Geophysical Monograph - American Geophysical Union, 2006).

70 Servali, A. & Korenaga, J. Oceanic origin of continental mantle lithosphere. *Geology* **46**, 1047-1050 (2018).

71 Stachel, T., Viljoen, K. S., Brey, G. & Harris, J. W. Metasomatic processes in lherzolitic and harzburgitic domains of diamondiferous lithospheric mantle: REE in garnets from xenoliths and inclusions in diamonds. *Earth and Planetary Science Letters* **159**, 1-12 (1998).

Used garnet Cr systematics to document high-P metamorphic origin of cratonic peridotites from low pressure melt residues.

72 Tainton, K. M. & McKenzie, D. The Generation of Kimberlites, Lamproites, and Their Source Rocks. *Journal of Petrology* **35**, 787-817 (1994).

73 Parman, S. W., Grove, T. L., Dann, J. C. & De Wit, M. J. A subduction origin for komatiites and cratonic lithospheric mantle. *South African Journal of Geology* **107**, 107-118 (2004).

74 Carlson, R. W., Pearson, D. G. & James, D. E. Physical, chemical, and chronological characteristics of continental mantle. *Reviews of Geophysics* **43**, doi:Rg100110.1029/2004rg000156 (2005).

75 Simon, N. S. C., Carlson, R. W., Pearson, D. G. & Davies, G. R. The origin and evolution of the Kaapvaal cratonic lithospheric mantle. *Journal of Petrology* **48**, 589-625, doi:10.1093/petrology/egl074 (2007).

76 Pearson, D. G. & Wittig, N. Formation of Archaean continental lithosphere and its diamonds: the root of the problem. *Journal of the Geological Society* **165**, 895-914, doi:10.1144/0016-76492008-003 (2008).

77 Pearson, D. G., Carlson, R. W., Shirey, S. B., Boyd, F. R. & Nixon, P. H. Stabilization of Archean Lithospheric Mantle - a Re-Os Isotope Study of Peridotite Xenoliths from the Kaapvaal Craton. *Earth and Planetary Science Letters* **134**, 341-357 (1995).

78 Walter, M. J. Melt extraction and compositional variability in the mantle. *In: Holland, H.D., Turekian, K.K. (Eds.), Treatise on Geochemistry, vol. 2. Elsevier, Amsterdam, pp. 363-394. Chapter 8.* (2003).

79 Bell, D. R. *et al.* Silica and volatile-element metasomatism of Archean mantle: a xenolith-scale example from the Kaapvaal Craton. *Contributions to Mineralogy and Petrology* **150**, 251-267, doi:10.1007/s00410-005-0673-8 (2005).

80 Ganne, J. & Feng, X. Primary magmas and mantle temperatures through time. *Geochemistry, Geophysics, geosystems* **18**, 872-888, doi:https://doi.org/10.1002/2016GC006787 (2017).

81 Pearson, D. G. & Wittig, N. The formation and evolution of the subcontinental mantle lithosphere - evidence from mantle xenoliths. Treatise of Geochemistry, Volume 3: The Mantle and Core, Chapter 3.6, 255–292. (2014).

82 Shu, Q. *et al.* The evolution of the Kaapvaal craton: A multi-isotopic perspective from lithospheric peridotites from Finsch diamond mine. . *Precambrian Research* **331**, 105380. (2019).
83 Su, B. & Chen, Y. Making cratonic lithospheric mantle. *Journal of Geophysical Research: Solid Earth* **123**, 7688-7706 (2018).
84 Gibson, S. A. & Mills, S. On the nature and origin of garnet in highly-refractory Archean lithospheric mantle: constraints from garnet exsolved in Kaapvaal craton orthopyroxenes. *Mineralogical Magazine* **81**, 781-809 (2017).
85 Canil, D. & Lee, C. T. A. Were deep cratonic mantle roots hydrated in Archean oceans? *Geology* **37**, 667-670, doi:10.1130/g25610a.1 (2009).
86 Schulze, D. J. Calcium anomalies in the mantle and a subducted metaserpentinite origin for diamonds. *Nature* **319**, 483-485 (1986).
Initial exploration of the idea of subducted precursors to deep cratonic roots
87 Perchuk, A. L., Gerya, T. V., Zakharov, V. S. & Griffin, W. L. Building cratonic keels in precambrian plate tectonics. *Nature* **586**, 395-401 (2020).
88 Regier, M. *et al.* An oxygen isotope test for the origin of Archean mantle roots. *Geochemical Perspectives Letters* **9**, 6-10 (2018).
89 Liu, J. *et al.* Mesoproterozoic plume-driven re-cratonisation of deep continental lithospheric mantle. *Nature* (2021 - in press).
90 Lee, C.-T. A. & Chin, E. J. Calculating melting temperatures and pressures of peridotite protoliths: Implications for the origin of cratonic mantle. *Earth and Planetary Science Letters* **403**, 273-286 (2014).
91 Scott, J. *et al.* Continent stabilisation by lateral accretion of subduction zone-processed depleted mantle residues; insights from Zealandia. *Earth and Planetary Science Letters* **507**, 175-186 (2019).
92 Brandon, A. D., Snow, J. E., Walker, R. J., Morgan, J. W. & Mock, T. D. Pt-190-Os-186 and Re-187-Os-187 systematics of abyssal peridotites. *Earth and Planetary Science Letters* **177**, 319-335, doi:10.1016/s0012-821x(00)00044-3 (2000).
93 Harvey, J. *et al.* Ancient melt extraction from the oceanic upper mantle revealed by Re–Os isotopes in abyssal peridotites from the Mid-Atlantic ridge. *Earth and Planetary Science Letters* **244**, 606-621, doi:10.1016/j.epsl.2006.02.031 (2006).
94 Kramers, J. D. Lead, uranium, strontium, potassium and rubidium in inclusion-bearing diamonds and mantle-derived xenoliths from southern Africa. *Earth and Planetary Science Letters* **42**, 58-70 (1979).
95 Menzies, M. & Murthy, V. R. Enriched mantle: Nd and Sr isotopes in diopsides from kimberlite nodules. *Nature* **283**, 634-636 (1980).
Along with Kramers (above) ad Richardson (below), pioneering studies defining the geochemical evidence for the longevity of crtaonic roots
96 Richardson, S. H., Gurney, J. J., Erlank, A. J. & Harris, J. W. Origin of diamonds in old enriched mantle. *Nature* **310**, 198-202 (1984).
97 Walker, R. J., Carlson, R. W., Shirey, S. B. & Boyd, F. R. Os, Sr, Nd, and Pb Isotope Systematics of Southern African Peridotite Xenoliths - Implications for the Chemical Evolution of Subcontinental Mantle. *Geochimica Et Cosmochimica Acta* **53**, 1583-1595 (1989).

98 Carlson, R. W. *et al.* in *The J.B. Dawson Volume, Proceedings of the VIIth International Kimberlite Conference* (eds J.J. Gurney, J.L. Gurney, M.D. Pascoe, & S.H. Richardson) 99-108 (Red Roof Design, 1999).

99 Griffin, W. L., Spetsius, Z. V., Pearson, N. J. & O'Reilly, S. Y. In situ Re-Os analysis of sulfide inclusions in kimberlitic olivine: New constraints on depletion events in the Siberian lithospheric mantle. *Geochemistry Geophysics Geosystems* **3**, doi:1069
10.1029/2001gc000287 (2002).

100 Irvine, G. J., Pearson, D. G. & Carlson, R. W. Lithospheric mantle evolution of the Kaapvaal Craton: A Re-Os isotope study of peridotite xenoliths from Lesotho kimberlites. *Geophysical Research Letters* **28**, 2505-2508, doi:10.1029/2000gl012411 (2001).

101 Rudnick, R. L. & Walker, R. J. Interpreting ages from Re-Os isotopes in peridotites. *Lithos* **112**, 1083-1095, doi:10.1016/j.lithos.2009.04.042 (2009).

102 Liu, J. *et al.* Mapping lithospheric boundaries using Os isotopes of mantle xenoliths: An example from the North China Craton. *Geochimica Et Cosmochimica Acta* **75**, 3881-3902, doi:10.1016/j.gca.2011.04.018 (2011).

103 Luguet, A. & Pearson, G. Dating mantle peridotites using Re-Os isotopes: The complex message from whole rocks, base metal sulfides, and platinum group minerals. *American Mineralogist* **104**, 165-189 (2019).

104 Griffin, W. L. *et al.* The world turns over: Hadean–Archean crust–mantle evolution. *Lithos* **189**, 2-15, doi:http://dx.doi.org/10.1016/j.lithos.2013.08.018 (2014).

105 Meibom, A. *et al.* Re-Os isotopic evidence for long-lived heterogeneity and equilibration processes in the Earth's upper mantle. *Nature* **419**, 705-708 (2002).

106 Pearson, D. G., Parman, S. W. & Nowell, G. M. A link between large mantle melting events and continent growth seen in osmium isotopes. *Nature* **449**, 202-205, doi:10.1038/nature06122 (2007).

107 Bragagni, A. *et al.* The geological record of base metal sulfides in the cratonic mantle: A microscale 187Os/188Os study of peridotite xenoliths from Somerset Island, Rae Craton (Canada). *Geochimica et Cosmochimica Acta* **216**, 264-285, doi:https://doi.org/10.1016/j.gca.2017.04.015 (2017).

108 van Acken, D. *et al.* Mesoarchean melting and Neoarchean to Paleoproterozoic metasomatism during the formation of the cratonic mantle keel beneath West Greenland. *Geochimica Cosmochimica Acta* **203**, 37-53 (2017).

109 Wainwright, A. N., Luguet, A., Fonseca, R. O. C. & Pearson, D. G. Investigating metasomatic effects on the 187Os isotopic signature: A case study on micrometric base metal sulphides in metasomatised peridotite from the Letlhakane kimberlite (Botswana). *Lithos* **232**, 35-48, doi:https://doi.org/10.1016/j.lithos.2015.06.017 (2015).

110 Beall, A. P., Moresi, L. & Cooper, C. M. Formation of cratonic lithosphere during the initiation of plate tectonics. *Geology* **46**, 487-490, doi:10.1130/g39943.1 (2018).

111 Doucet, L. S., Ionov, D. A. & Golovin, A. V. Paleoproterozoic formation age for the Siberian cratonic mantle: Hf and Nd isotope data on refractory peridotite

xenoliths from the Udachnaya kimberlite. *Chemical Geology* **391**, 42-55, doi:10.1016/j.chemgeo.2014.10.018 (2015).

112 Ionov, D. A., Liu, Z., Golovin, A. V., Korsakov, A. V. & Xu, Y. The age and origin of cratonic lithospheric mantle: Archean dunites vs. Paleoproterozoic harzburgites from the Udachnaya kimberlite, Siberian craton. *Geochimica Cosmochimica Acta* **281**, 67-90 (2020).

113 Liu, J. *et al.* Diamondiferous Paleoproterozoic mantle roots beneath Arctic Canada: A study of mantle xenoliths from Parry Peninsula and Central Victoria Island. *Geochimica et Cosmochimica Acta* **239**, 284-311 (2018).

114 Czas, J., Pearson, D. G., Stachel, T., Kjarsgaard, B. A. & Read, G. H. A Palaeoproterozoic diamond-bearing lithospheric mantle root beneath the Archean Sask Craton, Canada. *Lithos* **356**, 105301 (2020).

115 Luguet, A. *et al.* An integrated petrological, geochemical and Re-Os isotope study of peridotite xenoliths from the Argyle lamproite, Western Australia and implications for cratonic diamond occurrences. *Lithos* **112**, 1096-1108, doi:10.1016/j.lithos.2009.05.022 (2009).

116 Wittig, N. *et al.* Formation of the North Atlantic Craton: Timing and mechanisms constrained from Re-Os isotope and PGE data of peridotite xenoliths from SW Greenland. *Chemical Geology* **276**, 166-187, doi:10.1016/j.chemgeo.2010.06.002 (2010).

117 Griffin, W. L., Graham, S., O'Reilly, S. Y. & Pearson, N. J. Lithosphere evolution beneath the Kaapvaal Craton: Re–Os systematics of sulfides in mantle-derived peridotites. *Chemical Geology* **208**, 89-118, doi:10.1016/j.chemgeo.2004.04.007 (2004).

118 Schoene, B., de Wit, M. J. & Bowring, S. A. Mesoarchean assembly and stabilization of the eastern Kaapvaal craton: A structural-thermochronological perspective. *Tectonics* **27**, (10.1029) (2008).

119 Eglington, B. Evolution of the Namaqua-Natal Belt, southern Africa–A geochronological and isotope geochemical review. *Journal of African Earth Sciences* **46**, 93-111 (2006).

120 Janney, P. E. *et al.* Age, Composition and Thermal Characteristics of South African Off-Craton Mantle Lithosphere: Evidence for a Multi-Stage History. *Journal of Petrology* **51**, 1849-1890, doi:10.1093/petrology/egq041 (2010).

121 Eglington, B. M. & Armstrong, R. A. The Kaapvaal Craton and adjacent orogens, southern Africa: a geochronological database and overview of the geological development of the craton. *South African Journal of Geology* **107**, 13–32 (2004).

122 Mather, K. A., Pearson, D. G., McKenzie, D., Kjarsgaard, B. A. & Priestley, K. Constraints on the depth and thermal history of cratonic lithosphere from peridotite xenoliths, xenocrysts and seismology. *Lithos* **125**, 729-742, doi:10.1016/j.lithos.2011.04.003 (2011).

123 Ionov, D. A., Carlson, R. W., Doucet, L. S., Golovin, A. V. & Oleinikov, O. B. The age and history of the lithospheric mantle of the Siberian craton: Re–Os and PGE study of peridotite xenoliths from the Obnazhennaya kimberlite. *Earth and Planetary Science Letters* **428**, 108-119, doi:https://doi.org/10.1016/j.epsl.2015.07.007 (2015).

124 Pernet-Fisher, J. F. *et al.* Plume impingement on the Siberian SCLM: Evidence from Re-Os isotope systematics. . *Lithos* **218-219**, 141-154 (2015).

125 Liu, J. *et al.* Age and evolution of the deep continental root beneath the central Rae craton, northern Canada. *Precambrian Research* **272**, 168-184, doi:http://dx.doi.org/10.1016/j.precamres.2015.11.001 (2016).

126 Smit, K. V., Pearson, D. G., Stachel, T. & Seller, M. Peridotites from Attawapiskat, Canada: Mesoproterozoic Reworking of Palaeoarchaean Lithospheric Mantle beneath the Northern Superior Superterrane. *Journal of Petrology* **55**, 1829-1863, doi:10.1093/petrology/egu043 (2014).

127 Liu, J., Scott, J. M., Martin, C. E. & Pearson, D. G. The longevity of Archean mantle residues in the convecting upper mantle and their role in young continent formation. *Earth and Planetary Science Letters* **424**, 109-118, doi:http://dx.doi.org/10.1016/j.epsl.2015.05.027 (2015).

128 Kamber, B. S. & Tomlinson, E. L. Petrological, mineralogical and geochemical peculiarities of Archean cratons. *Chemical Geology* **511**, 123-151 (2019).

129 Cawood, P. A. *et al.* Accretionary orogens through Earth history 1-36 (Geological Society, London, Special Publications 2009).

130 Herzberg, C., Condie, K. & Korenaga, J. Thermal history of the Earth and its petrological expression. *Earth and Planetary Science Letters* **292**, 79-88, doi:10.1016/j.epsl.2010.01.022 (2010).

131 Li, X., Kind, R., Yuan, X., Wolbern, I. & Hanka, W. Rejuvenation of the lithosphere by the Hawaiin plume. *Nature* **427**, 827-829 (2004).

132 Sand, K. K. *et al.* The lithospheric mantle below southern West Greenland: A geothermobarometric approach to diamond potential and mantle stratigraphy. *Lithos* **112**, 1155-1166, doi:10.1016/j.lithos.2009.05.012 (2009).

133 Bernstein, S., Szilas, K. & Kelemen, P. B. Highly depleted cratonic mantle in West Greenland extending into diamond stability field in the Proterozoic. *Lithos* **168–169**, 160-172, doi:http://dx.doi.org/10.1016/j.lithos.2013.02.011 (2013).

134 Hamilton, M. A., Pearson, D. G., Thompson, R. N., Kelley, S. P. & Emeleus, C. H. Rapid eruption of Skye lavas inferred from precise U-Pb and Ar-Ar dating of the Rum and Cuillin plutonic complexes. *Nature* **394**, 260-263 (1998).

135 Nixon, P. H. Kimberlites in the south-west Pacific. *Nature* **287**, 718-720 (1980).

First study to recognise thick oceanic lithospheric mantle and deeply derived oceanic magmas

136 Ishikawa, A., Pearson, D. G. & Dale, C. W. Ancient Os isotope signatures from the Ontong Java Plateau lithosphere: Tracing lithospheric accretion history. *Earth and Planetary Science Letters* **301**, 159-170, doi:10.1016/j.epsl.2010.10.034 (2011).

137 Celli, N. L., Lebedev, S., Schaeffer, A. J. & Gaina, C. African cratonic lithosphere carved by mantle plumes. *Nature Communications* **11**, 92, doi:https://doi.org/10.1038/s41467-019-13871-2 (2020).

138 Ayalew, D. & Gibson, S. L. Head-to-tail transition of the Afar mantle plume: Geochemical evidence from a Miocene bimodal basalt–rhyolite succession in the Ethiopian Large Igneous Province. *Lithos* **112**, 461-476 (2009).

139 Capitanio, F. A., Nebel, O. & Cawood, P. A. Thermochemical lithosphere differentiation and the origin of cratonic mantle. *Nature* **588**, 89-94 (2020).

140 Moyen, J. F. & van Hunen, J. Short-term episodicity of Archaean plate tectonics. *Geology* **40**, 451-454 (2012).

141 Wang, H., van Hunen, J. & Pearson, D. G. Making Archean cratonic roots by lateral compression: A two-stage thickening and stabilization model. *Tectonophysics* **746,**, 562-571, doi:https://doi.org/10.1016/j.tecto.2016.12.001 (2018).

142 Oxburgh, E. R. & Parmentier, E. M. Thermal processes in the formation of continental lithosphere. *Philos Trans A Math Phys Eng Sci* **288**, 415-425 (1978).

143 Jordan, T. H. Structure and formation of the continental lithosphere. *In: M.A. Menzies and K. Cox (Editors), Oceanic and Continental Lithosphere; similarities and differences. J. Petrol., Special Lithosphere Issue, pp. 11-37.* (1988).

144 McKenzie, D., Jackson, J. & Priestley, K. Thermal structure of oceanic and continental lithosphere. *Earth and Planetary Science Letters* **233**, 337-349, doi:10.1016/j.epsl.2005.02.005 (2005).

145 McKenzie, D. & Priestley, K. Speculations on the formation of cratons and cratonic basins. *Earth and Planetary Science Letters* **435**, 94-104, doi:10.1016/j.epsl.2015.12.010 (2016).

146 Gray, R. & Pysklywec, R. N. Geodynamic models of mature continental collision: Evolution of an orogen from lithospheric subduction to continental retreat/delamination. *Journal of Geophysical Research: Solid Earth* **117** (2012).

147 Nicolas, A., Boudier, F. & Boullier, a. M. Mechanisms of flow in naturally and experimentally deformed peridotites. *american Journal of Science* **273**, 853-876 (1973).

Key study relating olivine flow in experiments, with real rock structures and seismic anisotropy

148 Liddell, M. V., Bastow, I. D., Darbyshire, F., Gilligan, A. & Pugh, S. The formation of Laurentia: Evidence from shear wave splitting. . *Earth and Planetary Science Letters* **479**, 170-178 (2017).

149 Priestley, K., Ho, T. & McKenzie, D. The formation of continetal roots. *Geology* **49**, doi:https://doi.org/10.1130/G47696.1 (2020).

150 Hoffman, P. F. United plates of America, the birth of a craton: Early Proterozoic assembly and growth of Laurentia. *Annual Reviews of Earth and Planetary Sciences* **16**, 543-603 (1988).

151 Percival, J. A. & Pysklywec, R. N. Are Archean lithospheric keels inverted? *Earth and Planetary Science Letters* **254**, 393-403, doi:10.1016/j.epsl.2006.11.047 (2007).

152 VanKranendonk, M. J., Smithies, R. H., Hickman, A. H. & Champion, D. C. Secular tectonic evolution of Archean continental crust: interplay between horizontal and vertical processes in the formation of the Pilbara Craton, Australia. *Terra Nova* **19**, 1-38 (2007).

153 Francheteau, J. *et al.* High heat flow in southern Tibet. *Nature* **32-36** (1984).

154 England, P. C. & Thompson, A. B. in *Collisional Tectonics* Vol. 19 (eds M. P. Coward & A. C. Reis) 83-94 (The Geological Society of London Special Publication, 1986).

155 Davis, W. J., Fryer, B. J. & King, J. E. Geochemistry and Evolution of Late Archean Plutonism and Its Significance to the Tectonic Development of the Slave Craton. *Precambrian Research* **67**, 207-241 (1994).

156 Peterson, T. D., Scott, J. M. J., LeCheminant, A. N., Jefferson, C. W. & Pehrsson, S. J. The Kivalliq Igneous Suite: Anorogenic bimodal magmatism at 1.75 Ga in the western Churchill Province, Canada. *Precambrian Research* **262**, 101-119, doi:http://dx.doi.org/10.1016/j.precamres.2015.02.019 (2015).

157 Weller, O. M., Copley, A., Miller, W. G. R., Palin, R. M. & Dyck, B. The relationship between mantle potential temperature and oceanic lithosphere buoyancy. *Earth and Planetary Science Letters* **518**, 86-99 (2019).

158 Rudnick, R. L. & Fountain, D. M. Nature and composition of the lower continentalL-crust - A lower crustal perspective. *Reviews of Geophysics* **33**, 267-309, doi:10.1029/95rg01302 (1995).

159 Reimink, J. R., Davies, J. H. F. L. & Ielpi, A. Global zircon analysis records a gradual rise of continental crust throughout the Neoarchean. *Earth and Planetary Science Letters* **554**, 116654 (2021).

160 Stern, T. A. *et al.* in *Continental Plate Boundary, Tectonics at South Island, New Zealand* Vol. 175 (eds D. O'kaya, T. Stern, & F. Davey) 207-233 (American Geophysical Union, Geophysical Monograph, 2007).

161 Chesley, J. T., Rudnick, R. L. & Lee, C. T. Re-Os systematics of mantle xenoliths from the East African Rift: Age, structure, and history of the Tanzanian craton. *Geochimica Et Cosmochimica Acta* **63**, 1203-1217, doi:10.1016/s0016-7037(99)00004-6 (1999).

162 Pearson, D. G., Irvine, G. J., Ionov, D. A., Boyd, F. R. & Dreibus, G. E. Re-Os isotope systematics and platinum group element fractionation during mantle melt extraction: a study of massif and xenolith peridotite suites. *Chemical Geology* **208**, 29-59, doi:10.1016/j.chemgeo.2004.04.005 (2004).

163 Alard, O., Griffin, W. L., Pearson, N. J., Lorand, J.-P. & O'Reilly, S. Y. New insights into the Re–Os systematics of sub-continental lithospheric mantle from in situ analysis of sulphides. *Earth and Planetary Science Letters* **203**, 651-663, doi:https://doi.org/10.1016/S0012-821X(02)00799-9 (2002).

164 Aulbach, S. *et al.* Mantle formation and evolution, Slave Craton: constraints from HSE abundances and Re–Os isotope systematics of sulfide inclusions in mantle xenocrysts. *Chemical Geology* **208**, 61-88, doi:10.1016/j.chemgeo.2004.04.006 (2004).

165 Korenaga, J. Urey ratio and the structure and evolution of Earth's mantle. *Reviews in Geophysics* **46** (2008).

166 Crameri, F., Shephard, G. E. & Heron, P. J. The misuse of colour in science communication. *Nature Communications* **11**, 5444 (2020).

Acknowledgements:

DGP is grateful for a Canada Excellence Research Chair that allowed the development of the data and ideas presented. A University of Otago, William Evans Visiting Fellowship was crucial to completing this manuscript. Modelling performed by LHW was funded by Research Council of Norway (Grant 280567). We thank Peter Cawood for constructive comments and John VanDecar for patience and encouragement.

Author contributions:

DGP wrote the manuscript, with major contributions to the various concepts covered by JS, TC, JL, AS, LHW, JvH, PK & KS. AS provided the seismology models, HLW performed the geodynamic models, augmented by JvH. JL performed the trace element modelling.

Competing interests:

The authors declare no competing interests.

DISPLAY ITEM CAPTIONS

Box 1 ***Craton definition and Earth's mantle lithosphere and crust-mantle relationships***

SEE FIGURE FOR BOX 1

Box 1a: Schematic depiction of Earth's mantle lithosphere defined here as the outer layer of Earth where heat is lost by conduction (the "tectosphere" of Jordan[2,14]). Geotherms depict pressure - temperature relations for thermally equilibrated lithosphere, with surface heat flow in mWm^{-2}. Depth to the base of the lithosphere is taken as the intersection of the conductive geotherm with the typical mid oceanic ridge (MOR) isentrope. Adjacent idealised cross section through northern Canada starting in the SE Slave craton (~ 60 °N) to the Sverdrup basin ~ 80 °N, with generalized locations of kimberlite fields and other magmatic rocks that provide constraints on lithospheric thickness through xenolith-derived mantle geotherms and magma geochemistry. Typical range in olivine compositions given as the fosterite content (Fo# in blue text). Lithospheric thickness varies between crust of different age, though lithospheric thicknesses of up to 200 km are present beneath crust of Proterozoic as well as Archean age[24,89,113] (See also Fig 1). Lithospheric thickness is much thinner beneath Phanerozoic continental crust and the oceans. **Box 1b:** 3-D perspective of the lithosphere beneath southern Africa showing the Archean nuclei and Paleo to Mesoproterozoic domains of the "Kalahari craton" that comprises the Kaapvaal and Zimbabwe Archean nuclei and intervening Paleo- to Mesoproterozoic regions. Location of kimberlite pipes supplying mantle xenolith data for lithosphere ages given by circles. Colour of circles denotes median age of lithospheric mantle (data from [57,74,77,98,120]). Crustal ages are representative only. Present day depth of lithosphere taken from seismology[25,74].

FIGURE 1 Seismic imaging of continental mantle lithosphere – defining cratonic regions. Global S-wave tomographic slice (oceans excluded) through Earth at 150 km depth displaying the wide-spread high wave-speed anomalies of deep cratonic mantle roots - in shades of blue - that extend far beyond the boundaries of the exposed/inferred crust of 55 identifiable Archean nuclei (% Vs anomalies relative to a modified AK135 reference model[24]). Cratons, with crust stable since ~ 1 Ga and underpinned by lithosphere > 150km thick occupy ~ 63% of the continental landmass. Asterix represents modified cratons where ancient crust is underlain by recently thinned lithosphere. Composite cratons comprise multiple Archean nuclei/cratons. The 5 Supercratons comprise multiple composite cratons. Diagonal stripes cover regions strongly influenced by subducting slabs and are not classified as cratons. For a 200 km tomographic slice, and a similar image coloured according to conventions for scientific maps, see Supplementary Material.

Box 2 ***Mantle peridotite density and mineralogy as a function of melt depletion***: Bulk density variation, as relative % change from a fertile (un-melted) mantle peridotite (lherzolite) as a function of fraction of melt extracted, for polybaric perfect fractional melting of 3 different pressures of melt initiation: 3 GPa, 5GPa and 7 GPa, following[33]. Green horizontal bars show the variation in residual (melt-depleted) peridotite mineralogy (for pyroxenes and olivine normalized to 100%) and hence lithological change, as extracted melt fraction increases. The most residual (melt-depleted) mantle peridotite is a dunite.

FIGURE 2: ***Estimating depth of melt extraction for lithospheric peridotites.*** Peridotite bulk rock molar Mg/Al ratio variation with bulk rock Yb concentration along with polybaric, perfect fractional melting curves for mantle melting beginning at different depths, following similar approaches to[67]. Residual mantle melting mineralogy variations with pressure and melt fraction from[36]. Melt fraction extracted (in wt. %) given along evolution lines for residual mantle. Data points shown for cratonic peridotites, data fields for oceanic mantle (abyssal and ocean island peridotites) and modified cratonic mantle, e.g., the eastern North China Craton. The majority of cratonic peridotites plot between the trends for melting beginning at 7 and 3 GPa melting, indicating typical starting melting pressures of 5 to 3 GPa. A much smaller fraction of cratonic peridotite residues, e.g., those form Artemisia[89] (north Slave craton) began melting at 7 GPa or deeper and are likely plume-derived melting residues.

Box 3 ***Dating lithospheric mantle: Lithospheric mantle age versus composition and relationship to crust***

General text: Os is a compatible element, remaining in the mantle residue during melt extraction[29,77,97]. Much higher Os concentrations in the melt-depleted peridotites versus any later metasomatic melts make Re-Os model ages more robust than many ages constraints on melting provided by incompatible element-based systems such as Rb-Sr, Sm-Nd and Lu-Hf, though the system is not immune from disturbance[101,103,161]. The use of whole rock platinum group element (PGE) patterns to evaluate later disturbance of peridotite Re-Os systematics by metasomatism[49,162] is essential. Emphasis is placed on ages from the most melt depleted, sulfide-absent peridotites, with the lowest Re and Pd concentrations. The advent of in-situ Re-Os dating of sulfides in peridotites[99,163,164], or mechanical extraction and dissolution of whole sulfides[107-109] increased the utility of Re-Os dating in peridotites, though sulfide should be absent in highly depleted peridotite compositions. For discussion of the relative merits of these approaches see[47,101,103].

Box 3 CAPTION: **Dating mantle melt depletion, mantle ages versus craton crust ages and evolution, age versus melt residue composition for mantle peridotites: A)** *Left panel* - Re-Os model age calculation assuming that during extensive (>25%) melt extraction from a peridotite, all Re goes into the melt, yielding a melt residue with Re/Os = 0. Extrapolation to a "mantle evolution curve" (black, blue and green lines – representing different models of mantle evolution) give "Re depletion model ages" (vertical axis). *Middle and right panels* - Probability density plots (bandwidth = 100 Myr) for melt depletion ages of mantle beneath cratons dominated by Archean crust (Archean cratonic mantle), Proterozoic cratons (Proterozoic cratonic mantle), Modified cratonic mantle (>1Ga crust with thin lithospheric roots, e.g., eastern North China craton, East Greenland), and Modern oceanic mantle (abyssal peridotites and Phanerozoic ophiolites). See Fig. 1 and text for craton classifications.
Far-right panel - Model continental growth curve[17] (green), plus (yellow shaded area) a moving average of the proportion of sediments with a given age distribution[159] for "mature sediment sources", with a relative age spread between the modal zircon U-Pb age and the age of the sediment of 0.4 (normalized to the age of the Earth at the time of deposition). Note the appearance of these mature sediments with the dramatic increase in cratonic mantle as documented Re-depletion ages.
B) Variation in olivine composition (box and whisker plots) in suites of mantle peridotites (single locations) versus Re-Os depletion age, where the most reliable age is based on combined Os - PGE systematics. Red boxes = mantle xenoliths erupted through crust of Archean nuclei, light-blue = mantle xenoliths erupted through crust of Proterozoic cratons, green = massif peridotites, deep-blue = Phanerozoic oceanic mantle. Note the occurrence of Archean mantle beneath Paleoproterozoic crust (e.g., locations 2 & 7) and Paleoproterozoic mantle beneath Archean crust (locations 16, 17, 19). Ages for locations where lithosphere formation is <100 Ma are given in arbitrary order in the expanded blue inset. Key to location numbers is given in the Supplementary Information. Salmon-coloured curves denote different present-day Urey ratio curves[165] (the ratio of internal heat generation in the mantle over the internal heat flux).

FIGURE 3: Geodynamic modelling of possible craton formation processes: Lateral compression and plume residue dispersal.

Panels A-B: Lateral compression (pure shear) model of Wang et al. [141] showing the lithosphere temperature and melt depletion fields at ~52 Myr (immediately after shortening) and at 503 Myr, after the start of the model. After initial compressional shortening the lithosphere thickens by cooling, becoming denser to the point where negative thermal buoyancy starts to exceed the inherent chemical buoyancy and results in further thickening. The melt depletion field is converted from the compositional field by assuming a maximum melt depletion of 35% for mantle peridotite.

Panels C-D: Dynamic model of plume upwelling tracking the path of melt residues. The temperature and melt depletion fields for residual peridotite comprising the lithospheric mantle keel shown at ~33 Myr and ~102 Myr after model initiation. Isotherms plotted at T=350 °C, 550 °C,900 °C,1300 °C. The calculation includes rheological strengthening due to melt depletion in the residual mantle. Note how the depleted plume residues rapidly disperse, partially accumulating beneath lithospheric traps, some being recycled back to the asthenosphere. Rheological strengthening due to melt depletion does not prevent plume melting residues from dispersing laterally by plume introduced flow, although a significant fraction of these buoyant residues remain in the uppermost mantle and may become accreted to craton roots during accretion or beneath much younger continents[91]. Model colours follow recommendations of [166] scientifically derived colour maps. Model details in Supplementary Methods.

On-line Methods

Numerical models

We use finite element code "Citcom" [167-169] to solve the thermochemical flow with extended Boussinesq approximation[170, 171]. A particle-tracking technique is used to track the movement of different chemical fields, including cratonic root and melt depletion. For detailed description of numerical method, including governing equations, rheology, and mantle plume setup, please refer to Wang et al. 2015[172]. The temperature plot is the model temperature after removing the adiabatic gradient, in order to make the plume clear in the temperature field.

We further include melting of mantle peridotite and depletion-dependent buoyancy and strengthening in the model. The anhydrous melting parameterization of [173] is used for mantle melting. The amount of melting is calculated for each particle, and any melt generated is removed immediately, assuming instantaneous extraction to the surface. The depletion field is updated with accumulated melting degree with each particle, which is then advected with particles just as with other chemical fields.

We apply an exponential change of mantle peridotite due to melt depletion[174]

$$\rho = \rho_0 exp(\alpha_d D)$$

where α_d defines the rate of density change due to melt depletion D. α_d =-0.0003 is used as reference value, which leads to 1.04% of density change at a melt depletion of 35%.

A composite rheology of non-Newtonian and Newtonian viscosity is used, with consideration of composition-dependent effects. The strengthening factor for the cratonic root and plume residue can be calculated as:

$$\Delta\eta = \Delta\eta_0^{min(1,\frac{C}{C_\eta})}$$

where C is the composition field, including cratonic root and melt depletion. C_η is the composition threshold for the maximum strengthening. A "constant strain-rate" definition is used for $\Delta\eta$, which would lead to an increase of non-Newtonian viscosity by $\Delta\eta^n$ in the definition of "constant stress"[172]. For depletion related rheological strengthening, we use a strengthening factor $\Delta\eta = 3$ in the reference model and vary $\Delta\eta$ between 1 and 10 in other models.

Model setup: The model domain is 2640 km wide and 660 km deep. A no-slip boundary condition is used on the top boundary, while other boundaries are at a free-slip condition. We use a total number of 384-by-96 elements with vertical mesh refinement at depth between 60 ~240 km depth. This provides a spatial resolution of 6.9 km by 4.3 km in this region. To track the composition field, ~1.7 million particles are used in the model domain, resulting in an average particle density of ~47 particles per element.

We start the models with a quasi-steady state thermal field that has ~100 km thick lithosphere. A hot plume with a maximum temperature anomaly of 250 ^{o}C rises up from the basal 660 km depth and the residual mantle from plume melting is produced and dispersed. The mantle potential temperature is 1550 ^{o}C, which leads to about 1800 ^{o}C at the base (660 km) due to adiabatic heating. However, the adiabatic thermal gradient is removed in Fig. 3C-D in order to emphasize the thermal anomaly introduced by the mantle plume.

Fig. 3C-D shows how the plume residue greatly disperses with the plume induced flow even with the rheological strengthening of 3 due to melt depletion. We varied the rheological strengthening factor from 1 to 10 and found that it did not prevent the dispersion of the residual mantle. The videos (PrTempDepletion.avi and PrTempVisc.avi) show the evolution of temperature, depletion, and viscosity field through time.

References

167. Moresi, L.-N. & Solomatov, V. S. Numerical investigation of 2D convection with extremely large viscosity variations. *Physics of Fluids* **7**, 2154–2162 (1995).
168. Zhong, S., Zuber, M. T., Moresi, L. & Michael, G. Role of temperature-dependent viscosity and surface plates in spherical shell models of mantle convection. *Journal of Geophysical Research* **105**, 11063–11082 (2000).
169. van Hunen, J., Zhong, S., Shapiro, N. M. & Ritzwoller, M. H. New evidence for dislocation creep from 3-D geodynamic modeling of the Pacific upper mantle structure. *Earth & Planetary Science Letters* **238**, 146–155 (2005).
170. Christensen, U. & Yuen, D. Layered convection induced by phase transitions. *Journal of Geophysical Research.* **90**, 10291–10300 (1985).
171. King, S. D. *et al.* A community benchmark for 2-D Cartesian compressible convection in the Earth's mantle. *Geophysical Journal* **180**, 73–87 (2010).
172. Wang, H., van Hunen, J. & Pearson, D. G. The thinning of subcontinental lithosphere: The roles of plume impact and metasomatic weakening. *Geochemistry, Geophysics & Geosystems* (2015). doi:10.1002/2015GC005784
173. Katz, R. F. A new parameterization of hydrous mantle melting. *Geochemistry Geophysics Geosystems* **4**, 1–19 (2003).
174. Schutt, D. L. & Lesher, C. E. Effects of melt depletion on the density and seismic velocity of garnet and spinel lherzolite. *Journal of Geophysical Research* **111**, B05401 (2006).

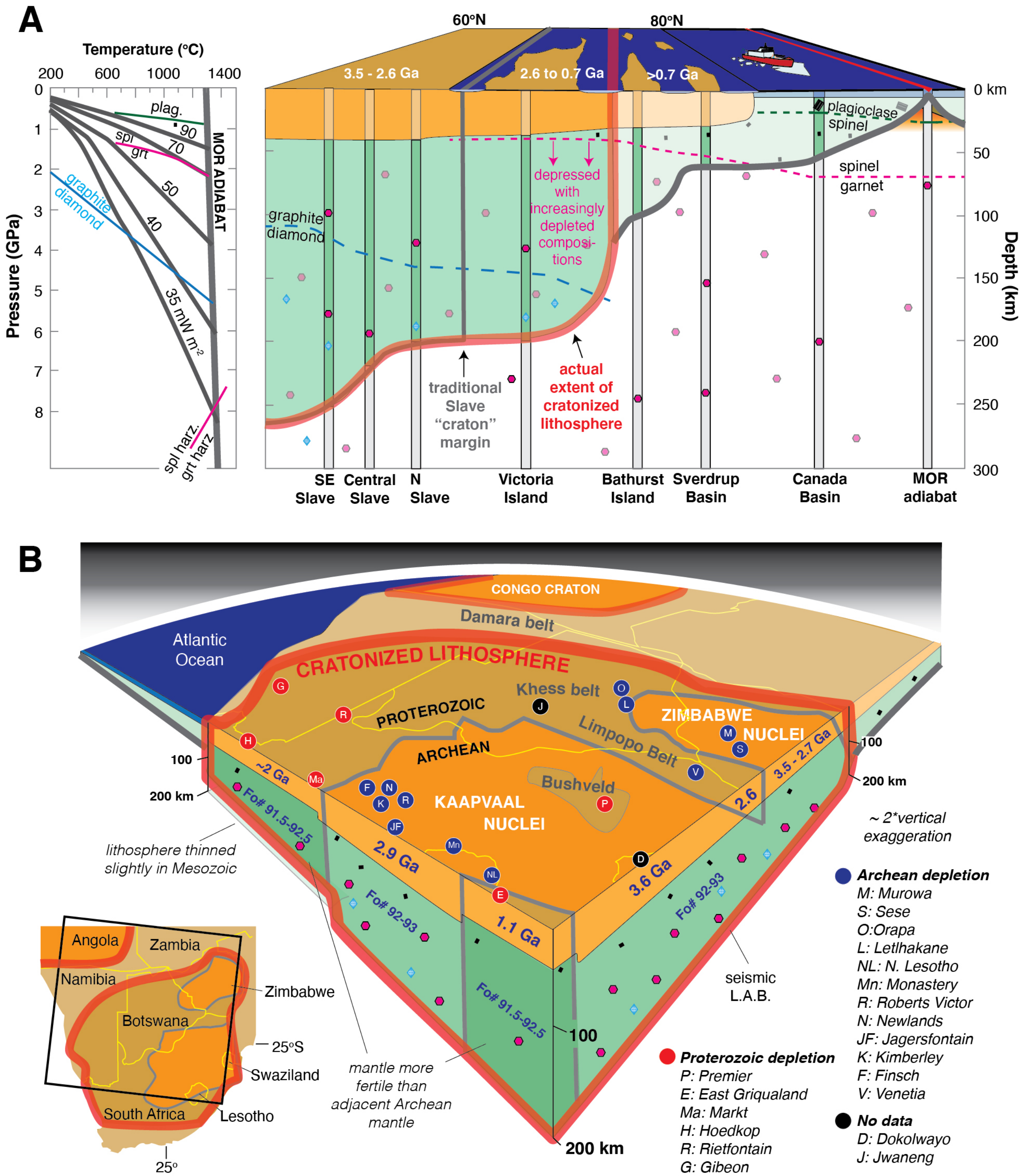

A
Temperature (°C)
200
600
1000
1400
Pressure (GPa)
plag.
spl
grt
90
70
50
40
35 mW m⁻²
graphite
diamond
MOR ADIABAT
spl harz.
grt harz
60°N
80°N
3.5 - 2.6 Ga
2.6 to 0.7 Ga
>0.7 Ga
0 km
plagioclase
spinel
spinel
garnet
Depth (km)
graphite
diamond
depressed
with
increasingly
depleted
compositions
traditional
Slave
"craton"
margin
actual
extent of
cratonized
lithosphere
SE Slave
Central Slave
N Slave
Victoria Island
Bathurst Island
Sverdrup Basin
Canada Basin
MOR adiabat
B
CONGO CRATON
Damara belt
Atlantic Ocean
CRATONIZED LITHOSPHERE
Khess belt
PROTEROZOIC
ARCHEAN
ZIMBABWE
NUCLEI
Limpopo Belt
KAAPVAAL
NUCLEI
Bushveld
~2 Ga
Fo# 91.5-92.5
2.9 Ga
Fo# 92-93
1.1 Ga
Fo# 91.5-92.5
3.6 Ga
Fo# 92-93
3.5 - 2.7 Ga
2.6
100
200 km
lithosphere thinned
slightly in Mesozoic
mantle more
fertile than
adjacent Archean
mantle
seismic
L.A.B.
~ 2*vertical
exaggeration
Angola
Zambia
Namibia
Zimbabwe
Botswana
25°S
Swaziland
South Africa
Lesotho
25°
Archean depletion
M: Murowa
S: Sese
O:Orapa
L: Letlhakane
NL: N. Lesotho
Mn: Monastery
R: Roberts Victor
N: Newlands
JF: Jagersfontain
K: Kimberley
F: Finsch
V: Venetia
Proterozoic depletion
P: Premier
E: East Griqualand
Ma: Markt
H: Hoedkop
R: Rietfontain
G: Gibeon
No data
D: Dokolwayo
J: Jwaneng

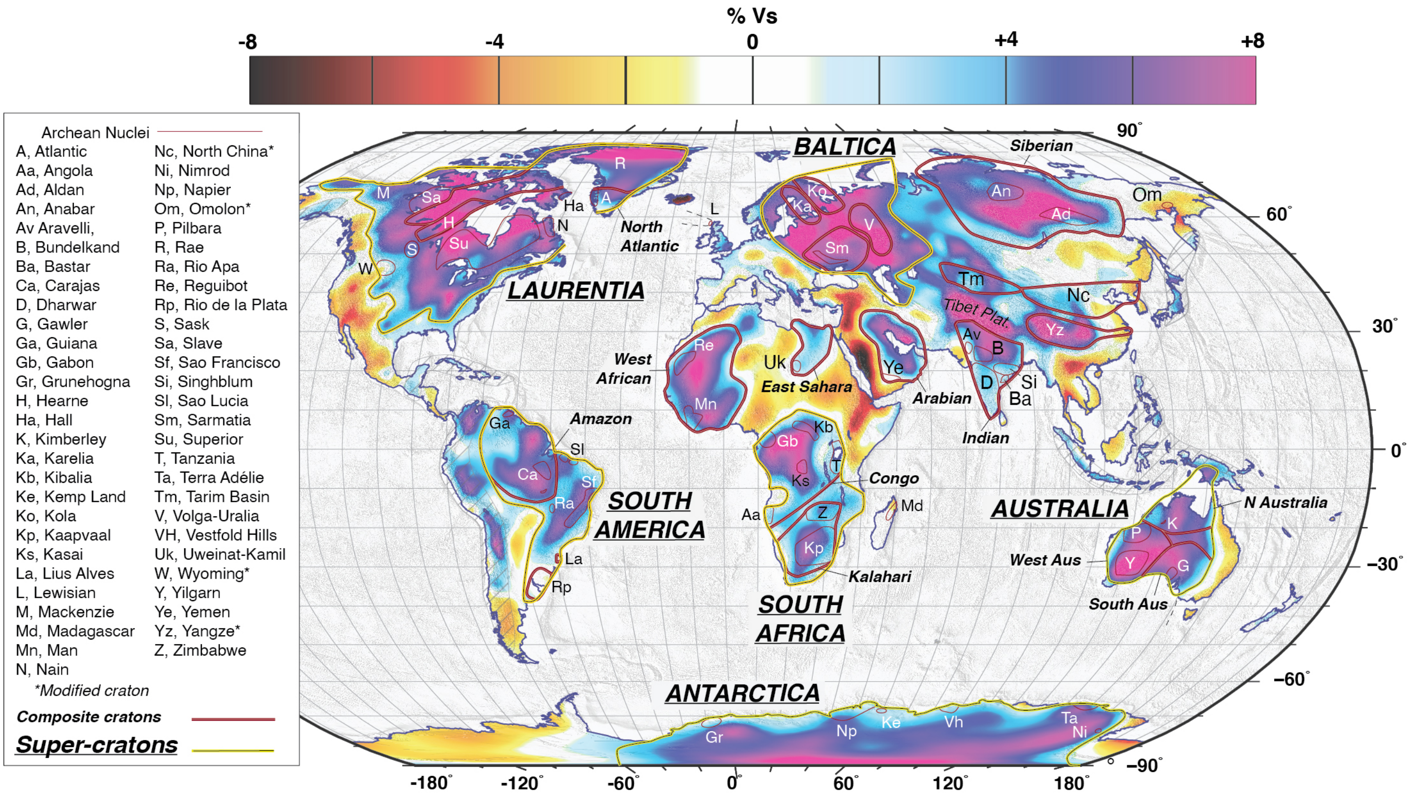
% Vs
-8
-4
0
+4
+8
Archean Nuclei
A, Atlantic
Aa, Angola
Ad, Aldan
An, Anabar
Av Aravelli,
B, Bundelkand
Ba, Bastar
Ca, Carajas
D, Dharwar
G, Gawler
Ga, Guiana
Gb, Gabon
Gr, Grunehogna
H, Hearne
Ha, Hall
K, Kimberley
Ka, Karelia
Kb, Kibalia
Ke, Kemp Land
Ko, Kola
Kp, Kaapvaal
Ks, Kasai
La, Lius Alves
L, Lewisian
M, Mackenzie
Md, Madagascar
Mn, Man
N, Nain
Nc, North China*
Ni, Nimrod
Np, Napier
Om, Omolon*
P, Pilbara
R, Rae
Ra, Rio Apa
Re, Reguibot
Rp, Rio de la Plata
S, Sask
Sa, Slave
Sf, Sao Francisco
Si, Singhblum
Sl, Sao Lucia
Sm, Sarmatia
Su, Superior
T, Tanzania
Ta, Terra Adélie
Tm, Tarim Basin
V, Volga-Uralia
VH, Vestfold Hills
Uk, Uweinat-Kamil
W, Wyoming*
Y, Yilgarn
Ye, Yemen
Yz, Yangze*
Z, Zimbabwe
*Modified craton
Composite cratons
Super-cratons
BALTICA
Siberian
LAURENTIA
North Atlantic
West African
East Sahara
Arabian
Indian
Tibet Plat.
Amazon
SOUTH AMERICA
Congo
Kalahari
SOUTH AFRICA
AUSTRALIA
N Australia
West Aus
South Aus
ANTARCTICA
90˚
60˚
30˚
0˚
−30˚
−60˚
−90˚
-180˚
-120˚
-60˚
0˚
60˚
120˚
180˚

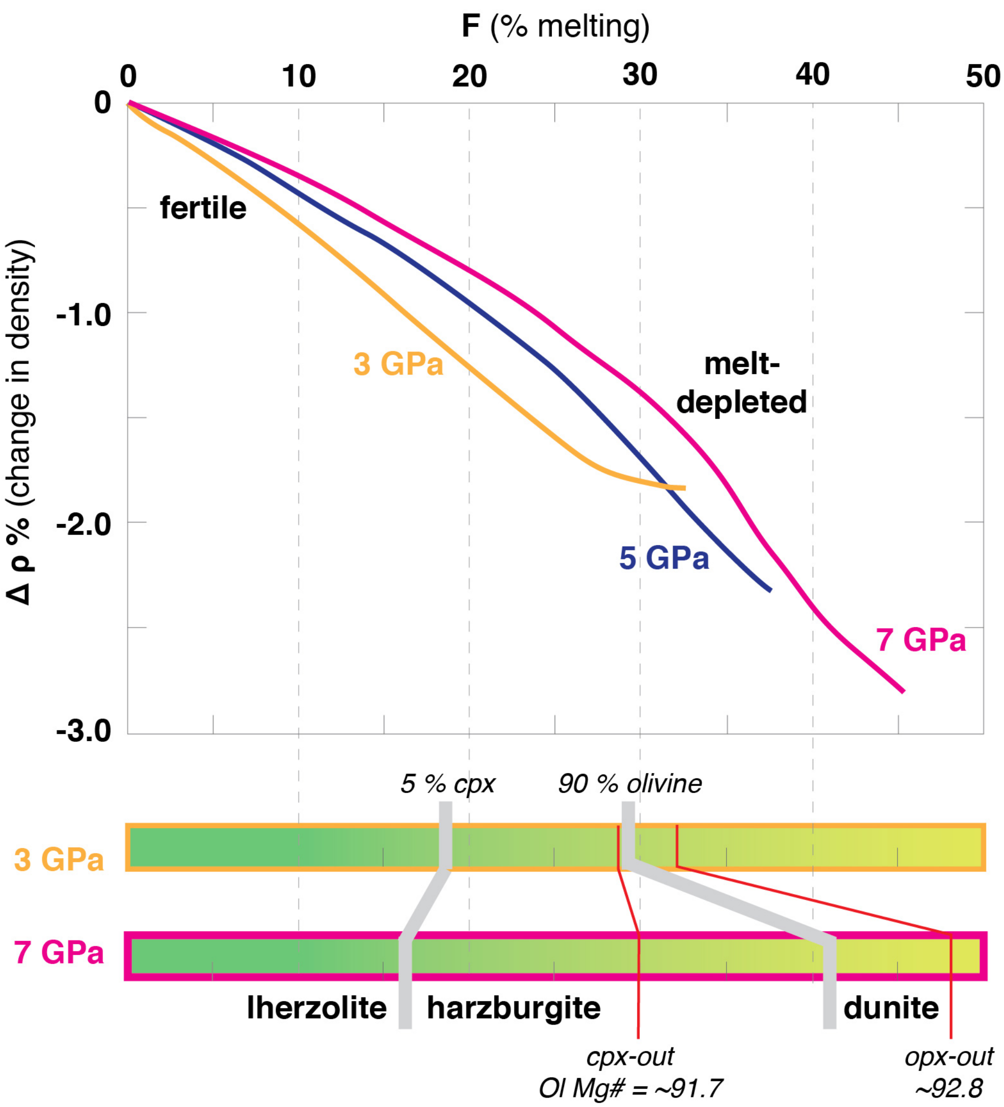

F (% melting)
0
10
20
30
40
50
0
-1.0
-2.0
-3.0
Δ ρ % (change in density)
fertile
3 GPa
melt-
depleted
5 GPa
7 GPa
5 % cpx
90 % olivine
3 GPa
7 GPa
lherzolite
harzburgite
dunite
cpx-out
Ol Mg# = ~91.7
opx-out
~92.8

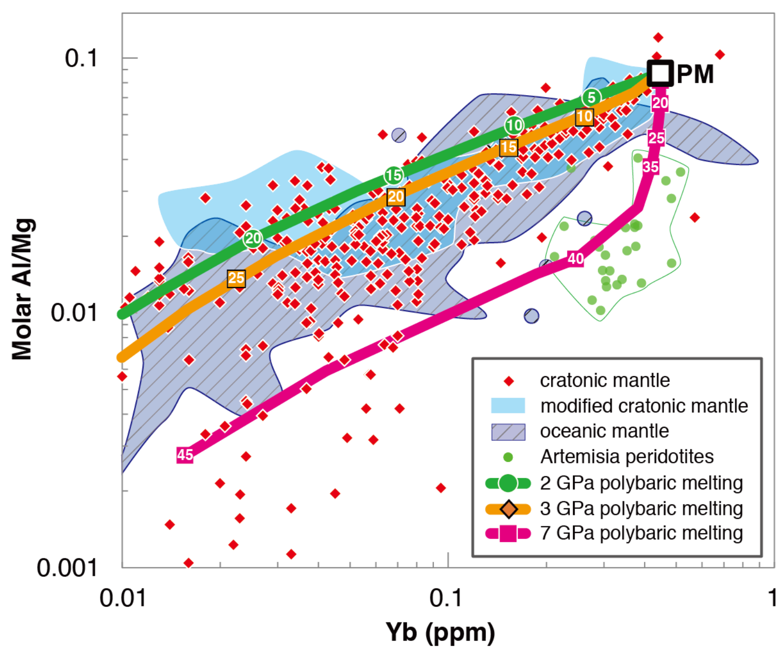

Molar Al/Mg
Yb (ppm)
0.1
0.01
0.001
0.01
0.1
1
PM
cratonic mantle
modified cratonic mantle
oceanic mantle
Artemisia peridotites
2 GPa polybaric melting
3 GPa polybaric melting
7 GPa polybaric melting
5
10
15
20
25
35
40
45

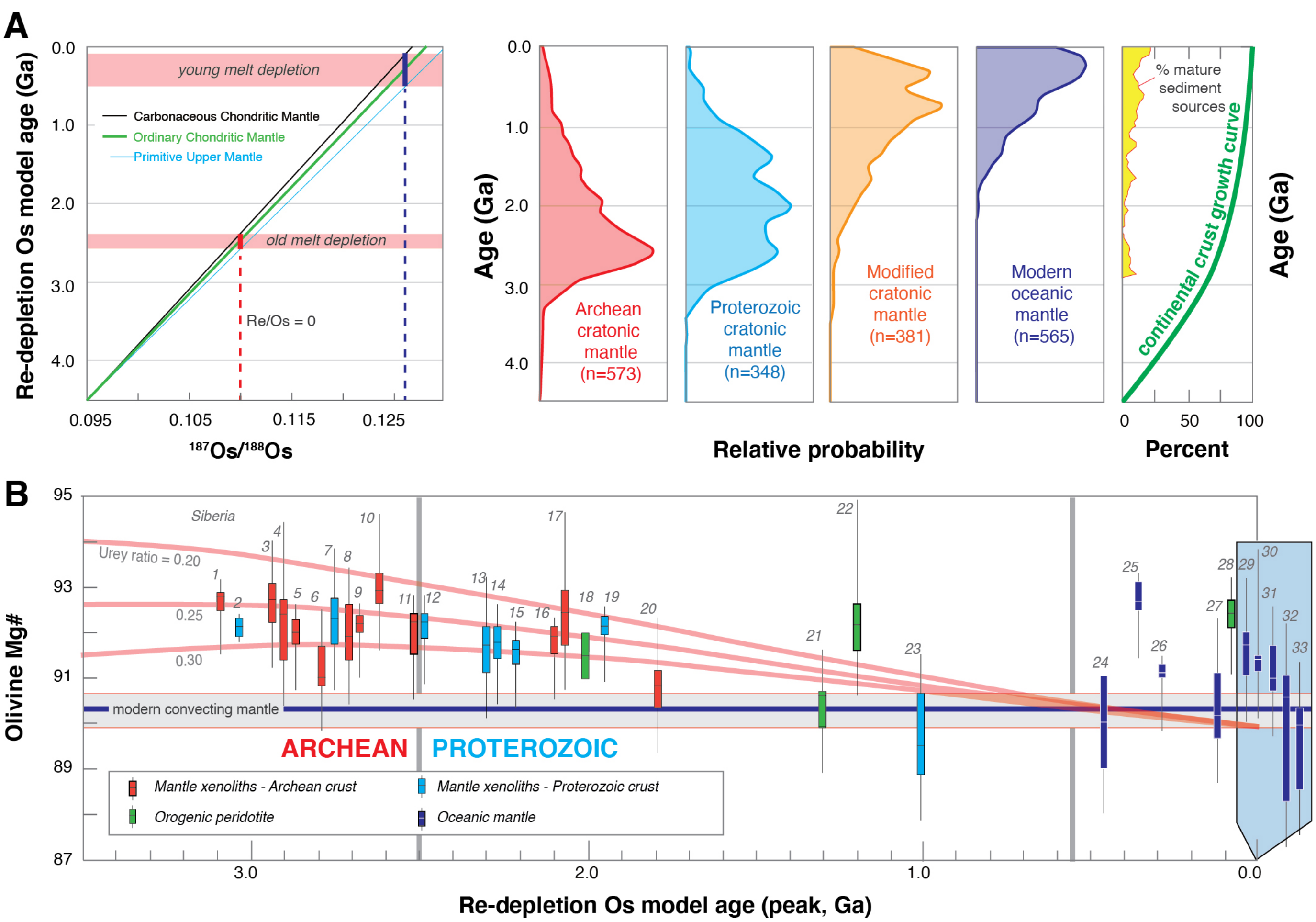
A
young melt depletion
old melt depletion
Carbonaceous Chondritic Mantle
Ordinary Chondritic Mantle
Primitive Upper Mantle
Re/Os = 0
Re-depletion Os model age (Ga)
$^{187}Os/^{188}Os$
Archean cratonic mantle (n=573)
Proterozoic cratonic mantle (n=348)
Modified cratonic mantle (n=381)
Modern oceanic mantle (n=565)
% mature sediment sources
continental crust growth curve
Age (Ga)
Relative probability
Percent
B
Siberia
Urey ratio = 0.20
0.25
0.30
modern convecting mantle
ARCHEAN
PROTEROZOIC
Mantle xenoliths - Archean crust
Mantle xenoliths - Proterozoic crust
Orogenic peridotite
Oceanic mantle
Olivine Mg#
Re-depletion Os model age (peak, Ga)

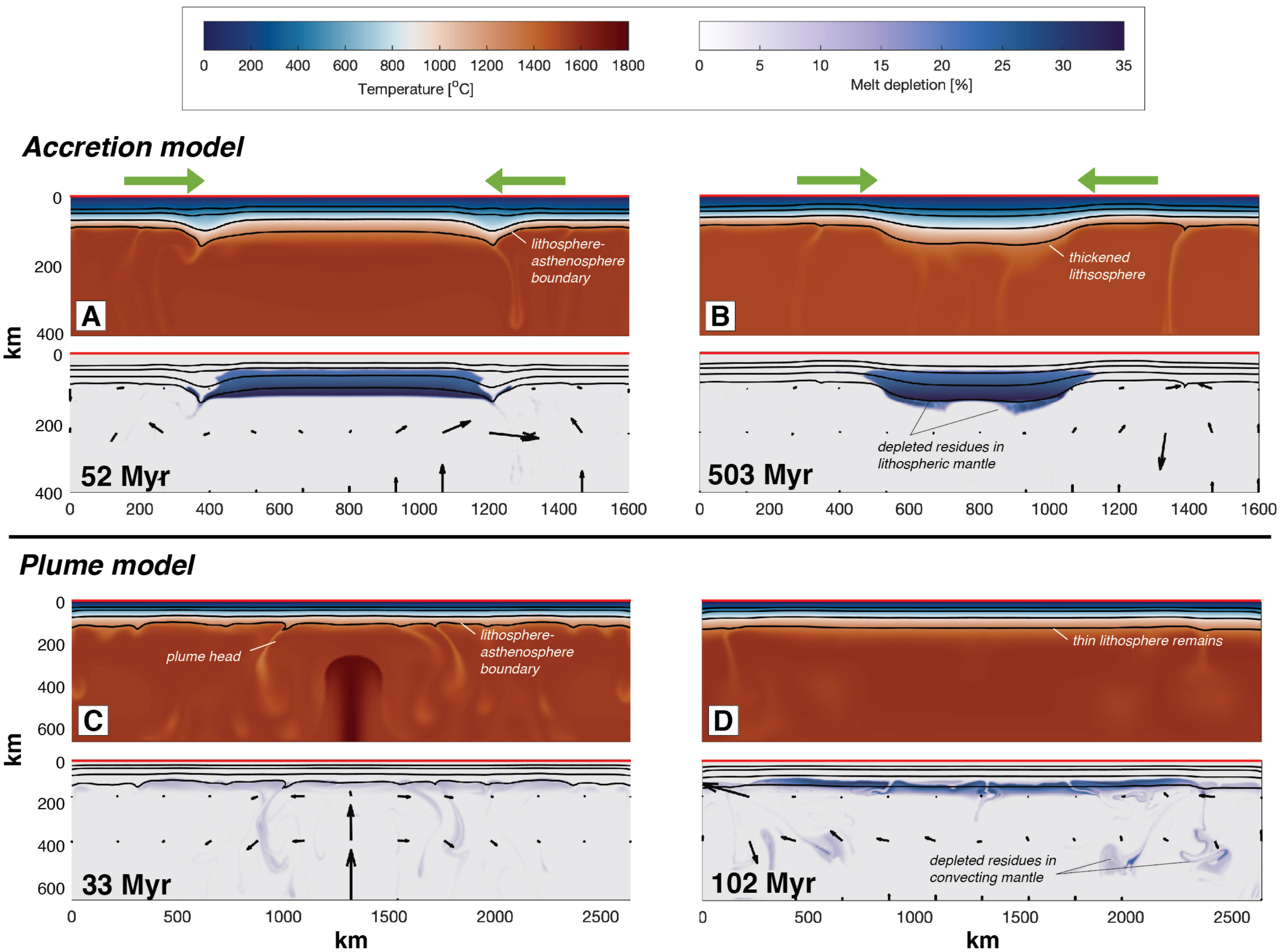

Temperature [°C]
Melt depletion [%]
Accretion model
lithosphere-asthenosphere boundary
thickened lithsosphere
depleted residues in lithospheric mantle
A
B
52 Myr
503 Myr
km
Plume model
plume head
lithosphere-asthenosphere boundary
thin lithosphere remains
depleted residues in convecting mantle
C
D
33 Myr
102 Myr
km

SI Guide

Supplementary Notes:
Supplementary Figures 1a & b and captions – a: Global seismic tomography section at 150km coloured according to recommendations for scientific maps; b: Regionalisation of lithospheric seismic properties.
Supplementary Location Notes to Box 3a (locations used in craton and oceanic age plots) & Box 3b (locations used in age versus Mg# plot).

Supplementary Videos (4)
LateralCompression_TempDepletion.avi
Video of dynamic model of lateral compression of cratonic mantle showing temperature and degree of melt depletion in the mantle. See "On-line Methods" for model methodology and caption to Figure 3 for further details.
LateralCompression_TempVisc.avi
Video of dynamic model of lateral compression of cratonic mantle showing temperature and viscosity in the mantle. See "On-line Methods" for model methodology and caption to Figure 3 for further details.
PlumeResidue_TempDepletion.avi
Video of the dynamics of the dispersion of mantle melting residues produced by mantle plumes showing temperature and extent of melt depletion in the mantle. See "On-line Methods" for model methodology and caption to Figure 3 for further details.
PlumeResidueTempVisc.avi
Video of the dynamics of the dispersion of mantle melting residues produced by mantle plumes showing temperature and viscosity in the mantle. See "On-line Methods" for model methodology and caption to Figure 3 for further details.

SUPLLEMENTARY NOTES

Supplementary Figure 1a: Seismic imaging of continental mantle.

Global S-wave tomographic slice (oceans excluded) through the Earth at 150 km depth. The scale bar displays % Vs anomalies relative to a modified AK135 reference model [References 23 and 24 of the main manuscript]. Colour scale is the "Vik" scheme derived using the recommendations for colour scales on maps [Reference 166 of the main manuscript].

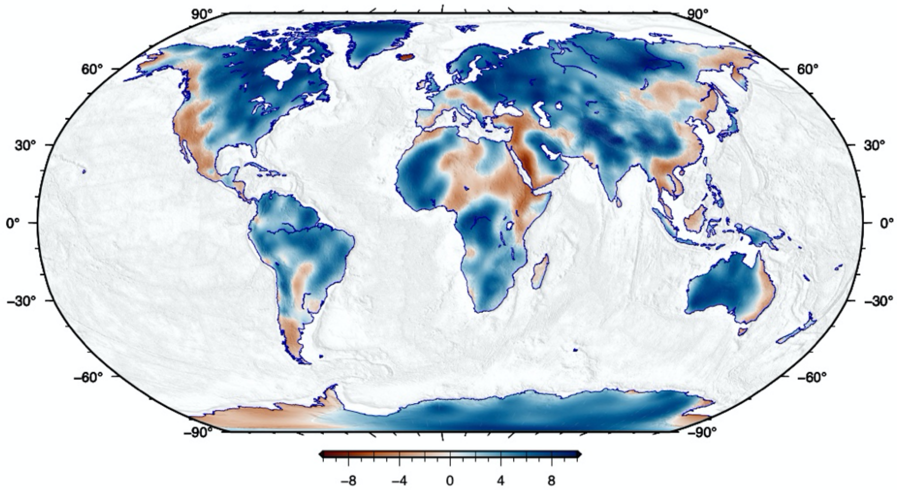

Supplementary Figure 1b : Seismic tectonic regionalisation of lithosphere.

Tectonic regionalisation [using the method of reference 23 – Main Manuscript] of the seismic data to objectively classify seismic velocities into regions of similarity within the Earth's upper mantle; falling out naturally from this is the division of continents from oceans (not shown), and the subdivision of continents into cratonic very deep lithosphere (green) that broadly coincides with the Archean crustal nuclei to cratons, cratonic deep lithosphere (150 km thick or more – blue colour), broadly coinciding with the Super-cratons and Composite cratons defined in Fig. 1 of the main manuscript, and non-cratonic mantle underpinned by lithospheric mantle extending to <150km to the lithosphere-asthenosphere boundary (grey shading). Diagonal stripes cover regions with apparent thick lithosphere that are strongly influenced by subducting slabs and are not classified as cratons. The boundaries of the ***cratons as a whole,*** as defined as the edges of the blue shaded regions, underpinned by lithosphere > 150km thick, ***comprise 63% of the total continental landmass***. ***Cratonic nuclei*** with the deepest lithospheres, from this classification occupy ***~ 34% of the total continental landmass***.

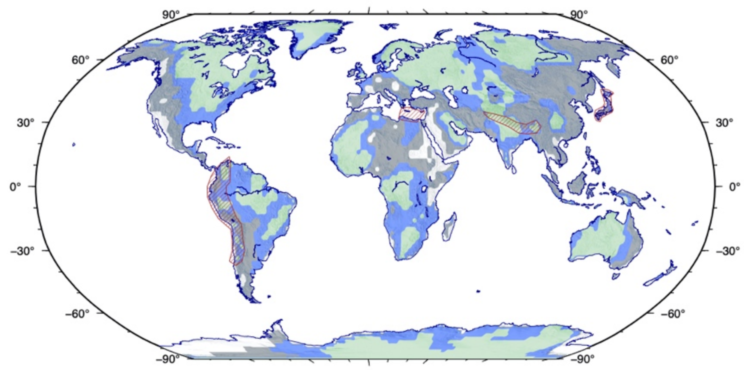

Box 3a: Locations grouped by type of craton in Re-Os model age compilation

Names are either the name of a given mine, or the location of the host kimberlite, lamproite or basalt

Archean Cratonic Mantle:

Kalahari craton Archean nuclei – Letseng Mine, Lhiqhobong Mine, Matsoku, Mothae Mine, Thaba Putsoa, Newlands Mine, Monastery Mine, Kimberley Mines (Bultfontein), Jagersfontein Mine, Finsch Mine, Murowa Mine.
Karelian craton – Kaavi, Kaavi-Kupio
Rae craton – Somerset Island, Repulse Bay, Pelly Bay, Darby
Slave craton – Jericho Mine, Diavik Mine, Ekati Mine, Artemisia, Gahcho Kué
North Atlantic Craton – Chidliak Mine (Baffin Island), Safartoq (W. Greenland), Nigerlikasik and Pyramidefjeld (W. Greenland)
Superior craton – Attawapiskat
Eastern North China craton – Fuxian, Mengyin (Pre-lithosphere thinning kimberlites).
Wyoming craton – Eagle buttes, Williams
Sask craton – Fort a la Corne

Proterozoic Cratonic Mantle

Kalahari composite craton – Venetia Mine, Orapa Mine, Lethlakane, Namaqua-Natal terrane kimberlites (Ramatseliso, East Griqualand, Abbotsford, Melton Wold, Uintjiesberg, Markt, Hebron, Hoedkop, Gansfontein, Klipfontein), Rehoboth terrane kimberlites (Gibeon field)
Congo composite craton – Usagaran terrane (Labait, Tanzania)
Western Australian composite craton – Argyle Mine
Laurentia Super-craton – Mackenzie craton (Parry Peninsula), Victoria Island; Hearne Terrane (Buffalo Head Hills), Central Plains Orogen (Sloan)
South American Super-craton - Alto Paranaiba
Siberian composite craton – Udachnaya Mine, Obnazhennaya

Modified Cratonic Mantle

South East Siberia – Tok
East China craton – Longquanlongwan, Kuandian, Hanuoba, Qixia, Yangyuan, Jining, Datong, Fansi, Fushan, Hebi, Dalongwan, Penglai, Shanwang, Baekryeong Island, Jeju Island, Pyeongtaek
Colorado Plateau - Big Creek
Mojavia – Cima
West Greenland – Ubekent Ejland
East Greenland - Wiedemann Fjord

Phanerozoic Oceanic Mantle (Abyssal, Arcs, Ophiolites)

Abyssal – Mid Atlantic Ridge Hole 1274A (ODP Leg 209), Kane Fracture Zone, SW Indian and American-Antarctic Ridges, MAR 15 20 FZ Cruise: Academic Boris Petrov, SWIR Atlantic II FZ Cruise: Robert Conrad 27-9, SWIR Du Toit FZ Cruise: Protea 5, Gakkel ridge (Arctic Ocean), Lena Trough, Arctic basin, Mid Atlantic Ridge (MAR) Saint Paul Fracture Zone
Ophiolites – Tiebaghi massif, New Caledonia; Ouassë Bay, New Caledonia; Me Maoya massif, New Caledonia; Massif du Sud, New Caledonia; Poum, New Caledonia; Babouillat, New Caledonia; Poum, New Caledonia; Babouillat, New Caledonia; Kopeto, New Caledonia; Mamonia complex, Cyprus, Troodos, Cyprus; Oman Ophiolite, Shetland Ophiolite, Taitao ophiolite; southern Chile, Koycegiz,

Turkey; Tekirova, Turkey, Marmaris, Turkey; Macquarie Island, Australia, Ligurian ophiolites, Italy; Totalp, Austria; Purang ophiolite, southwestern Tibet; Central Tibet - Bangong-Nuijang suture zone; Yarlung-Zangbo ophiolite, Tibet;
Arcs – Kamchatka (Bakening, Avachinsky, Valovayam; Cascade arc (Simcoe); Japan arc (Ichinomegata); SW Japan (Kurose); Bismark Archipelago (PNG); Izu-Bonin-Mariana Forearc, Conical seamount.

Box 3b: Locations plotted on Age versus olivine composition plot

1) Siberia (Udachnaya, Archean samples, plus Obnazhennaya)
2) Argyle, Australia
3) Kalahari craton - Kaapvaal nucleus (excluding Kimberley & Premier)
4) Tanzania craton
5) Kalahari Craton - Kaapvaal nucleus (Kimberley)
6) Wyoming craton
7) North Atlantic Craton (E, W. and SW Greenland)
8) Slave craton
9) Congo craton
10) Kalahari Craton - Zimbabwe nucleus (Murowa-Sese)
11) North China craton (Archean samples)
12) Rae craton - Somerset Island
13) Kalahari craton - East Griqualand
14) Kalahari craton - Namaqualand
15) Kalahari craton - Namibia
16) Kalahari Craton - Kaapvaal nucleus (Premier)
17) Siberia (Udachnaya, Proterozoic samples)
18) Pyrenees orogenic massifs
19) Parry Peninsula & Victoria Island
20) North China Craton (Post-Archean samples)
21) Ronda Massif, Spain
22) China - Songshugou
23) San Carlos - USA
24) Bay of Islands Ophiolite
25) Iwanadake ophiolite, Japan
26) Dun Mountain ophiolite, New Zealand
27) Ontong Java Plateau, Pacific Ocea
28) Anita peridotite, New Zealand
29) Mariana Arc, Pacific Ocean
30) Kamchatka, Russia
31) South Sandwich Islands, S. Atlantic Ocean
32) Lihir Island, Papua New Guinea
33) Japan arc-related mantle xenoliths - various locations